THE ASTROPHYSICAL JOURNAL, 467:370–384, 1996 August 10

HUBBLE SPACE TELESCOPE OBSERVATIONS OF ISOLATED PULSARS

G. G. PAVLOV,[1] G. S. STRINGFELLOW,[2] AND F. A. CÓRDOVA[3]
Pennsylvania State University, Department of Astronomy & Astrophysics, 525 Davey Laboratory, University Park, PA 16802-6305;
pavlov@astro.psu.edu, guy@casa.colorado.edu
Received 1995 October 31; accepted 1996 February 29

ABSTRACT

Using the COSTAR corrected Faint Object Camera on the *Hubble Space Telescope*, we have obtained deep ultraviolet and optical images of the fields containing three nearby radio pulsars spanning a range in age between $\sim 1 \times 10^5$ and 2×10^7 yr. Deep $7''.4 \times 7''.4$ images were obtained in the long-pass F130LP filter for the youngest, PSR B0656+14, and the oldest, PSR B0950+08, pulsars; each of the images contains only one pointlike source which is likely the UV-optical counterpart of the corresponding pulsar. PSR B1929+10 was imaged in the F130LP, F342W (U), and F430W (B) filters, and it was apparently detected in the former two images. The AB magnitudes in the F130LP filter are $m_{130LP} =$ 25.2, 27.1, and 26.9 for B0656+14, B0950+08, and B1929+10, respectively. For B1929+10 we also obtained $m_U = 26.8$ and $m_B > 26.2$. Comparison of the flux observed from B0656+14 with *ROSAT* data and model spectra of neutron star atmospheres shows that it is predominantly of a nonthermal origin, exceeding by several orders of magnitude predictions from phenomenological theoretical models. We predict that the thermal component of the flux should be observable in the far-UV domain. The fluxes observed from the older pulsars B0950+08 and B1929+09 are consistent with the assumption that they are thermal-like fluxes arising from the entire neutron star surface. Under this assumption, the observed (blackbody) temperature of B0950+08 is $T_\infty^{bb} = (7 \pm 1) \times 10^4$ K for the distance $d = 127 \pm 13$ pc and the neutron star radius $R_\infty = 13$ km. The fluxes observed from B1929+10 correspond to $T_\infty^{bb} = (1\text{–}3) \times 10^5$ K for the distance and interstellar extinction in the ranges $d = 150\text{–}180$ pc and $E(B-V) = 0.0\text{–}0.1$. These relatively high temperatures for the old pulsars require (re)heating mechanisms to be operating in old neutron stars. They can be explained by frictional heating due to dissipation of energy of differential rotation. The deep exposures set very stringent upper limits on the temperatures of neutron stars at these distances if our candidates are not the pulsars. For example, the field around B0950+08 has a 3 σ limit corresponding to 2×10^4 K at $d = 130$ pc.

Subject headings: pulsars: general — pulsars: individual (PSR B0656+14, PSR B1929+10, PSR B0950+08) — stars: evolution — stars: neutron

1. INTRODUCTION

Optical, ultraviolet, and soft X-ray radiation can be produced by a pulsar via both nonthermal emission by ejected/accreted relativistic particles and thermal emission from the neutron star (NS) surface. Investigation of the *nonthermal* radiation permits the physical conditions in pulsar magnetospheres to be probed, and the emission mechanisms operating in the pulsars to be ascertained. Although it has been more than 25 yr since pulsars were discovered, an unequivocal theory of pulsar emission still does not exist. Except for a few special cases, virtually all of our knowledge about the nonthermal radiation results from data in the radio and, for a few pulsars, X-ray and γ-ray domains. Additional ultraviolet and optical data can provide new insights into the origin and nature of the radiation, and assist with either discriminating between current models or constructing a new one.

It is also crucial to investigate the *thermal* radiation component. Since cooling of the NS depends essentially on its mass, radius, magnetic field, and especially on still poorly known properties of the superdense matter in NS interiors, measuring the surface temperatures of NSs of various ages would be invaluable in elucidating, in particular, the equation of state of matter at supranuclear densities and properties of nucleon superfluidity. Detection of the thermal radiation from young ($\tau \lesssim 10^4$ yr) pulsars is unlikely because their nonthermal radiation is so much more intense, as demonstrated by the example of the Crab pulsar ($\tau \simeq 10^3$ yr), for which only an upper limit of the surface temperature has been obtained (Becker & Aschenbach 1995). According to the theories of NS cooling, effective surface temperatures of *middle-aged* ($10^4 \lesssim \tau \lesssim 10^6$ yr) NSs are expected to be in the range of 10^5–10^6 K. NSs with such temperatures ($kT \sim 10$–100 eV) are most luminous in the extreme-ultraviolet (EUV), soft X-ray range. EUV detectors are still not very sensitive, and EUV radiation is strongly attenuated by the interstellar medium. Soft X-ray observations of middle-aged pulsars revealed that indeed at least four of them, PSR B0833−45 (Vela; $\tau = 1.1 \times 10^4$ yr), PSR B0656+14 ($\tau = 1.1 \times 10^5$ yr), Geminga ($\tau = 3.4 \times 10^5$ yr), and PSR B1055−52 ($\tau = 5.3 \times 10^5$ yr) emit thermal radiation from the NS surface with temperatures $\sim(3\text{–}10) \times 10^5$ K (Ögelman 1995). However, interpretation of these observations is not completely certain. In particular, fitting the observed spectra with NS atmosphere models (Pavlov et al. 1995) yields systematically lower (by a factor of 1.5–2.5, depending on the magnetic field and chemical composition) effective temperatures than the traditional

[1] On leave from A. F. Ioffe Physico-Technical Insititute, St. Petersburg, Russia.
[2] Present address: Center for Astrophysics and Space Astronomy of Colorado, Campus Box 389, Boulder, CO 80309-0389.
[3] Currently on leave at NASA headquarters.

blackbody fits. Such a difference in temperatures is very important for the comparison with the cooling theories; the different temperatures correspond to quite different cooling scenarios and different models of the NS interiors. To firmly evaluate the effective temperature, it is important to investigate the NS thermal radiation in another frequency domain, particularly in the UV-optical range. Although the nonthermal radiation could dominate the optical spectrum in the middle-aged pulsars, its flux is expected to decrease toward shorter wavelengths, and the thermal component could dominate somewhere in the UV. Since predicted UV fluxes are extremely faint, $U \gtrsim 26$–27 for the maximum brightness of the thermal component (Anderson et al. 1993; Meyer, Pavlov, & Mèszàros 1994), and the most promising far-UV range is unobservable from the ground, such observations can only be carried out at this time with the *Hubble Space Telescope* (*HST*).

After a few million years of their lives, *old* NSs would have already cooled to less than 10^5 K and would continue cooling unless additional mechanisms operate to produce heat. In particular, frictional interaction of the more rapidly rotating interior superfluid with the outer solid NS crust dissipates the energy of the differential rotation, heating the star (Van Riper, Link, & Epstein 1994, and references therein). For instance, the largest plausible values of the differential angular momentum of the frictionally coupled superfluid layers can provide $T \sim (1$–$2) \times 10^5$ K at an NS age of $\sim 10^7$ yr. Among other heating mechanisms, nucleon decay catalyzed by superheavy magnetic monopoles (e.g., Kolb & Turner 1984) should be mentioned. If the (unknown) monopole flux is high enough, very old NSs may even become hotter with time. Thus, measuring the temperatures of old NSs would allow, for instance, the efficiency of frictional dissipation to be evaluated, important for understanding still uncertain details of the interaction of the superfluid vortices with the crust lattice, and an estimate of the monopole flux to be obtained, important for elementary particle physics and cosmological models of the early universe. The temperature expected for the old NSs lies below the soft X-ray range, and the objects are too faint to be detected with modern EUV or ground-based optical telescopes, so that optical-UV observations of the old NSs with the *HST* is the best way to trace their thermal evolution.

The only pulsar for which IR, optical, and UV radiation has been studied in detail (Percival et al. 1993, and references therein) is the famous Crab pulsar (PSR B0531+21). Recently, two more young ($\tau \simeq 10^3$ yr) pulsars, PSR B0540−69 and PSR B1509−58, have been detected in the V band (Caraveo et al. 1992; Caraveo, Mereghetti, & Bignami 1994b). The youngest middle-aged (or the oldest young) Vela pulsar (PSR B0833−45) was detected in the B and U bands (Peterson et al. 1978, and references therein). In all four cases the radiation is definitely of a nonthermal origin. A number of attempts to detect optical radiation from older pulsars (e.g., Kristian 1970; Manchester et al. 1978; Bignami, Caraveo, & Vacanti 1988b; Perriman et al. 1989) proved to be unsuccessful; only upper limits $V \sim 21.5$–25 were established. An optical counterpart of the γ-ray source Geminga was identified by Halpern & Tytler (1988) and Bignami, Caraveo, & Paul (1988a) long before *ROSAT* observations of the object proved it to be a soft X-ray and γ-ray middle-aged pulsar (Halpern & Holt 1992; Bertsch et al. 1992; Halpern & Ruderman 1993). The optical identification was due to deep imaging of the *Einstein* HRI error box by several groups (see Bignami et al. 1987, and references therein). The optical magnitudes of this object, $R = 25.5 \pm 0.3$, $V = 25.4 \pm 0.2$, and $B \sim 26.5$ (Bignami et al. 1988a) seem to indicate a nonthermal origin of its optical radiation.[4] A marginal detection ($V \sim 25$) of PSR B0656+14 with a ground-based telescope has been reported quite recently by Caraveo, Bignami, & Mereghetti (1994a).

Utilizing the available soft X-ray data, we selected a sample of middle-aged and moderately old, relatively nearby pulsars and proposed observations in different spectral bands with the UV-sensitive Faint Object Camera (FOC) on board *HST*. The primary goals of this program were the following:

1. To detect UV-optical radiation from middle-aged and old pulsars;
2. To obtain spectrophotometry in several UV-optical wave bands in order to characterize the spectral shape, enabling the thermal and nonthermal components to be separately identified if the spectrum is composite;
3. If the radiation is of a thermal origin, to estimate various NS atmospheric parameters (effective temperature, etc.) to assist in discriminating between different theoretical NS cooling scenarios and to gain further insight into the properties of NS matter;
4. If the observed spectrum is nonthermal, to understand the nature of this radiation, and how its intensity depends on the pulsar parameters (age, period and its time derivative, magnetic field, etc.).

Our original proposal was scaled down substantially by the TAC, allowing us to pursue our goals only partly. Four hours were awarded for observations of three pulsars: the middle-aged pulsar PSR B0656+14 ($\tau = 1.1 \times 10^5$ yr), and the two older pulsars PSR B0950+08 ($\tau = 3 \times 10^6$ yr) and PSR B1929+10 ($\tau = 1.7 \times 10^7$ yr). A summary of the known properties of these pulsars is provided in Table 1. All of the pulsars had been previously detected in the soft X-ray range (B0656+14 is one of the brightest pulsars detected by *ROSAT*) and are relatively nearby objects (B0950+08 was the closest known pulsar at the time when the proposal was submitted). Conservative estimates of the expected fluxes forced us to plan observations of each pulsar for the time allocated with only one long-pass filter F130LP ($\lambda\lambda = 2310$–4530 Å) to maximize the possibility of detection. This required us to employ positional coincidence between the observed *HST* and radio positions to assist with identification of the UV-optical pulsar candidates. However, observations of our first two pulsars led us to observe our last, B1929+10, in two additional filters (see § 2). We believe all three pulsars were detected; for B0656+14, the radiation is mainly of a nonthermal origin, while for the other two pulsars the radiation is likely to be thermal. A detailed description of the observations and their reduction are given in § 2, while the analysis and interpretation of the observations are presented in § 3. Following a short summary of our findings, some implications are discussed in § 4.

Reports of this work during earlier stages have been given by Córdova, Stringfellow, & Pavlov (1994) and

[4] Recent *HST* observations (Bignami et al. 1996) confirmed the V magnitude and yielded additionally $U = 24.9 \pm 0.2$.

TABLE 1

PULSAR CHARACTERISTICS

PSR[a]	P (ms)	$\dot{P}$ (10^{-15})	Age (Myr)	B[b] (10^{12} G)	DM[c]	d (pc)	$\dot{E}$[d]	l (deg)	b (deg)	F_{400}[e] (mJy)
B0656+14.....	385	55.0	0.11	4.7	14	760[f] 200–500[g]	38	201.1	8.3	6
B0950+08.....	253	0.23	17.3	0.25	2.97	130[h]	0.56	228.9	43.7	400
B1929+10.....	227	1.16	3.1	0.51	3.18	170[f] 30–80[i] >250[j]	3.89	47.4	−3.9	250

[a] B0656+14 ≡ J0659+1414, B0950+08 ≡ J0953+0755, B1929+10 ≡ J1932+1059.
[b] Magnetic field $B = (3Ic^3P\dot{P}/8\pi^2R^6)^{1/2}$, for $R = 10^6$ cm, $I = 10^{45}$ g cm^2.
[c] Dispersion measure in cm^{-3} pc.
[d] Spin-down "luminosity," $\dot{E} = 4\pi^2 I\dot{P}P^{-3}$, in 10^{33} ergs s^{-1} (for $I = 10^{45}$ g cm^2).
[e] Energy flux at 400 MHz in mJy (= 10^{-26} ergs s^{-1} cm^{-2} Hz^{-1}).
[f] Dispersion measure based distance (Taylor et al. 1993).
[g] Distance estimate from *ROSAT* data (Finley et al. 1992; Anderson et al. 1993).
[h] The distance is $d = 127 \pm 13$ pc from parallax measurements (Gwinn et al. 1986).
[i] From parallax measurements by Salter et al. 1979.
[j] Lower limit from parallax measurements by Backer & Sramek (1982).

Stringfellow, Pavlov, & Córdova (1994). The results presented here supersede those of the earlier reports.

2. OBSERVATIONS AND DATA REDUCTION

Observations were conducted with the FOC early during cycle 4, just after the COSTAR corrective optics system was deployed. The FOC is a two-dimensional photon-counting imaging camera which is sensitive to radiation between $\lambda\lambda$1150–6500. The in-orbit dark noise is typically ~0.0007 counts s^{-1} pixel^{-1}. In normal mode the detector area is imaged with 512 × 512 resolution elements (pixels) at 16 bit length each, while in zoomed format the image area increases to 512z × 1024, but at 8 bit length, thereby decreasing the dynamic range. We employed the FOC + COSTAR in the f/96 mode; with COSTAR in place, this corresponds to an actual focal ratio of f/151, with 0.″0144 pixel^{-1} and imaging an area of 7.″4 × 7.″4 of the sky in normal mode, and 14.″7 × 14.″7 in 512z × 1024 (zoomed) mode.

Three fields containing the radio pulsars B0656+14, B0950+08, and B1929+10 were imaged with the long-pass filter F130LP. The primary goal of our program was to render detections of the pulsars, and since we did not know what characteristics the radiation emanating from the pulsars might have, this filter was selected due to its wide spectral coverage (FWHM ~ 2200 Å), high total throughput efficiency (up to 6.3%), and a sharp Lyα cutoff to avoid excessive airglow (see Fig. 1). Since the objects were expected to be extremely faint, the fields were imaged during *HST* nighttime to further minimize the airglow background. As the targets lie at low ecliptic latitudes (−8.°5, −4.°6, and 32.°3, respectively) where the zodiacal light is rather bright, the images were also taken during seasons when the ecliptic longitudes of the targets (105°, 145°, and 297°, respectively) are sufficiently far from the longitude of the Sun. Details of the observations are contained in Table 2.

We were allocated three orbits for each pulsar field. The dark-time constraint limited the maximum exposure time to 1655 s per orbit, and with the initial acquisition setup resulted in an exposure time of only 1445 s in the first orbit. This yielded a total exposure time in the summed F130LP images of 4755 s for the first two pulsars observed, B0656+14 and B0950+08. For each image, standard processing with the STScI FOC Routine Science Data Processing System (hereafter pipeline) which included a geometric distortion correction (GEO) applied to the raw image, followed by flat-fielding (UNI). The GEO corrects

TABLE 2

HST FOC/96 PULSAR OBSERVATIONS

Pulsar Candidate PS (1)	Filter (2)	Date (UT) (3)	Exposure (s) (4)	Radius[a] (pixels) (5)	Source[b] (counts) (6)	Sky[c] (counts pixel^{-1}) (7)	S/N (8)	Net[d] (counts) (9)	Count rate C_{tot} (counts s^{-1}) (10)	Flux[e] $\bar{F}_\nu$ (11)
B0656+14.....	F130LP	1994 Feb 17	4755[f]	6	3596 ± 69	5.23	52	4566	0.96 ± 0.02	30.5 ± 0.6
B0950+08.....	F130LP	1994 Apr 24	4755[f]	3	417 ± 27	5.50	15	738	0.16 ± 0.01	5.1 ± 0.3
B1929+10.....	F130LP	1994 Jul 10	1221	3	138 ± 15	1.48	9	244	0.20 ± 0.02	6.4 ± 0.6
B1929+10.....	F342W	1994 Jul 10	3310[g]	3	96 ± 15	2.17	6.5	170	0.052 ± 0.008	7.0 ± 1.1
B1929+10.....	F430W	1994 Jul 10	596	1.7	<17	0.76	<3	<44[h]	<0.074[h]	<12[h]

[a] Optimal pixel radius chosen to maximize signal-to-noise ratio for source counts.
[b] Background-subtracted source counts with 1σ uncertainties in a circle with the radius noted.
[c] Total (sky + dark noise) median background for summed exposure.
[d] Source counts incorporating encircled energy corrections based on PSF.
[e] Mean energy flux in units of 10^{-31} ergs cm^{-2} s^{-1} Hz^{-1}.
[f] Sum of three dark time exposures (1445 + 1655 + 1655 s).
[g] Sum of two dark time exposures (1655 + 1655 s).
[h] 3 σ upper limit.

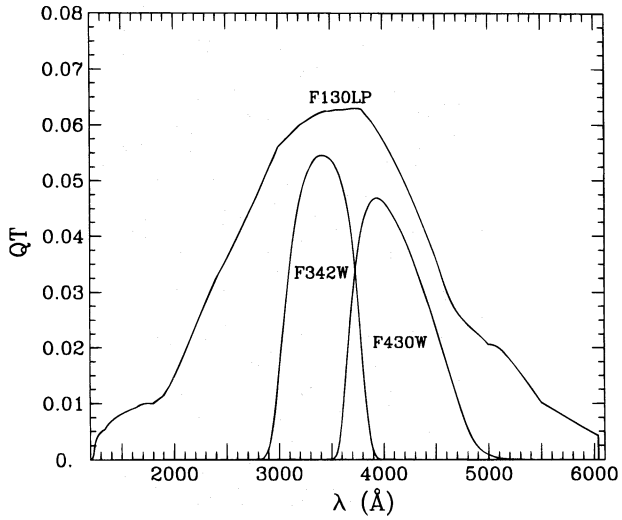

FIG. 1.—Total throughputs (OTA + COSTAR + filter + FOC) for the configurations used in our observations.

for both optical and detector distortion; the STScI file utilized for the standard format mode images was e1a1351fx.r5h. The F130LP filter is very broad, encompassing radiation from the UV through the visual part of the spectrum where the detector provides the red cutoff, so the appropriate flat field to use depends on the spectral characteristics of the source. The middle-aged and old pulsars can be expected to be UV bright compared to the optical. Therefore, of the four science-grade (smoothed, full image) flat fields available for the FOC, we selected the "UV" flat field constructed from various pointings of the Orion nebula (the only externally observed flat field) using the F140W filter (central wavelength 1370 Å). The pipeline file is c2410530x.r2h (hereafter C24), and all reported photometry results from the use of this UNI correction in the analysis, unless noted otherwise. However, for comparative quantitative assessment purposes we have also carried out analysis with the "blue" (central wavelength 4800 Å) internally constructed flat field with the file name bb1e14193.r2h (hereafter C1H), as this is the flat field selected by the pipeline based on the closest matching filter pivot wavelengths. The effect of the flat-field choice on the photometry is discussed in § 3.3.

The GEO and UNI (C24) corrected and summed images performed with the F130LP filter are shown in Figure 2 (Plate 4), each with a 7″.4 × 7″.4 field of view. Inspection of the images for the first two pulsars observed (B0656 + 14 in frame *a*, and B0950 + 08 in frame *b*) shows *only one pointlike source* near the image center, marked with an arrow, and one extended object located in the right upper corner of the image in each case. Our analysis has shown (see § 3) that the detected pointlike objects are very likely to be the pulsar counterparts. Moreover, due to precautions taken, the background in the exposures is indeed very low, virtually coinciding with the dark-time noise of the detector, and the signal-to-noise ratios (S/N) for the detected objects are unnecessarily high. Consequently, the statistical uncertainties of the source fluxes are, in fact, less than the possible systematic uncertainties associated, e.g., with flat-fielding. On the other hand, since the sky in the direction to B1929 + 10 is much more crowded, an additional color information may be needed to discriminate the pulsar among other field objects. We therefore modified the setup for then forthcoming observations of B1929 + 10: with assistance from the FOC team, our allocated time was split into two full dark orbits with the FOC "U" filter (F342W, central wavelength 3410 Å), a 20 minute observation with the F130LP filter, and a 10 minute observation in the FOC "B" filter (F430W, central wavelength 3940 Å). We chose to conduct the F430W observation in zoomed format mode to provide a wider field of view useful for astrometric analysis. The total throughputs of all the filters are shown in Figure 1.

The image for B1929 + 10 conducted in the F130LP filter (Fig. 2*c*) is indeed rich in comparison with the other two pulsar fields: seven objects are detected and labeled in Figure 2*c*. Objects 4–6 have not been detected in either the F342W (Fig. 3*a* [Pl. 5]) or F430W (Fig. 3*b*) images. Along with objects 1–3, nine additional objects are detected in the F430W image with its larger field of view, including a $V \sim 13$ mag star. The most likely pulsar candidate (see § 3) is marked by an arrow in Figure 2*c*. Notice that this object is also detected in the F342W image, but not in the F430W image.

3. ASTROMETRIC AND PHOTOMETRIC ANALYSIS

3.1. *Radio Positions*

To evaluate the probability that the pointlike sources are indeed the pulsar counterparts, we collected and analyzed the results of the radio astrometry of the pulsars. The most recent and reliable results on the positions and proper motions of the pulsars are summarized in Table 3. The most probable radio positions at the epochs of the *HST* observations, together with the FOC positions of the proposed pulsar counterparts, are presented in Table 4.

B0656 + 14.—The radio coordinates of B0656 + 14 result from timing observations by Dewey et al. (1988) and Arzoumanian et al. (1994), and from VLA observations by Thompson & Córdova (1994). The original data of Dewey et al. and Thompson & Córdova were presented for equinox B1950. We converted them to J2000 using a standard procedure described by Aoki et al. 1983, with allowance for the fact that the E terms of aberration were not included in the original coordinates determined by Dewey et al., but were included in those presented by Thompson & Córdova; both sets are in the FK4 system. The proper motion of this object was determined by Thompson & Córdova (1994) based on three sets of VLA observations (epochs 1989.07, 1990.38, and 1992.98). We reanalyzed the observational data and obtained slightly different values for the proper motion, which are presented in Table 3 (original values in Thompson & Córdova are $\mu_\alpha = +64 \pm 11$ mas yr^{-1}, $\mu_\delta = -28 \pm 4$ mas yr^{-1}). The revised proper motion was used to compute the radio position of B0656 + 14 (Table 4) at the epoch of our FOC observation (1994.13) starting from the most recent (and accurate) VLA position (epoch 1992.98). The uncertainties of the radio position (0″.09 and 0″.03 for α and δ, respectively) do not include possible systematic errors associated with the 1992.98 VLA coordinates. A thorough analysis of the pulsar position relative to the background radio sources revealed offsets, after correcting for the pulsar's proper motion, of typically 0″.2 in each of the three epochs, and that the positions of the background sources also varied by up to this amount relative to their positions at other epochs. This is likely due to

1996ApJ...467..370P

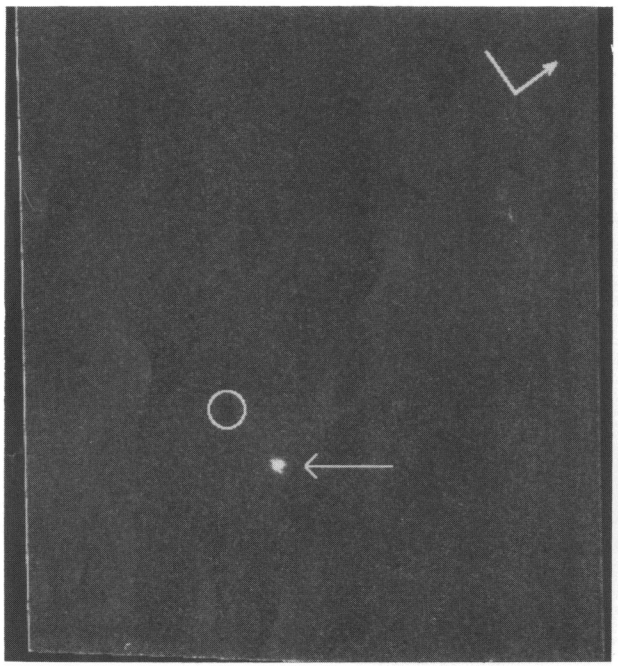

FIG. 2a

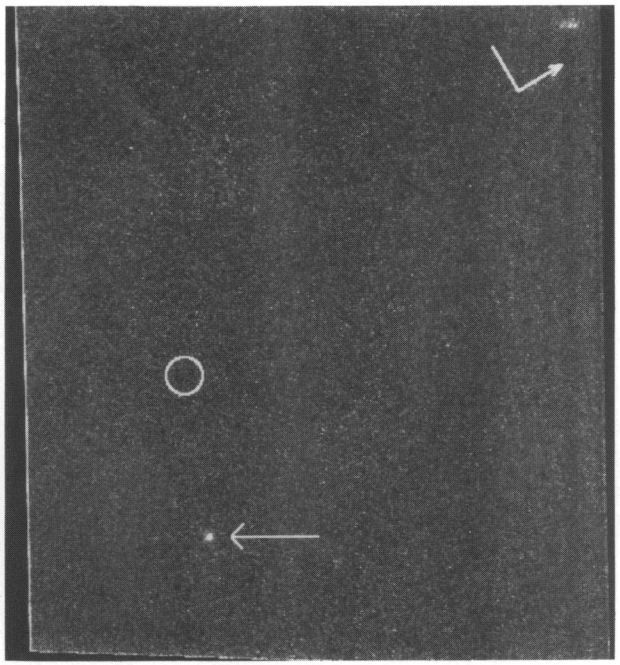

FIG. 2b

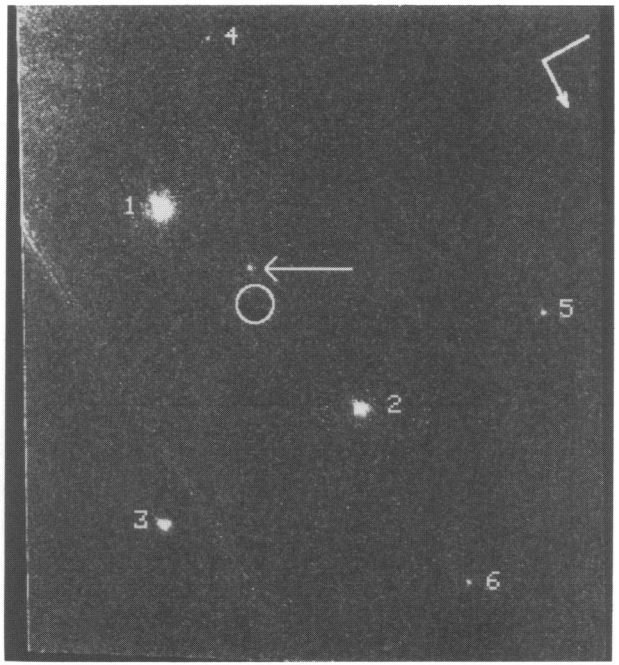

FIG. 2c

FIG. 2.—*HST* FOC images with the F130LP filter for (*a*) PSR B0656+14, (*b*) PSR B0950+08, and (*c*) PSR B1929+10. Each frame is 7.″4 × 7.″4 with the north-east orientation shown in the upper right corner, where north is shown with the arrow. The circles, which are 0.″2 in radius, indicate the pulsar radio positions at the epoch of our observations, and the arrows point to our candidate UV-optical pulsar counterparts. Details on the field objects labeled in frame (*c*) are provided in Table 5.

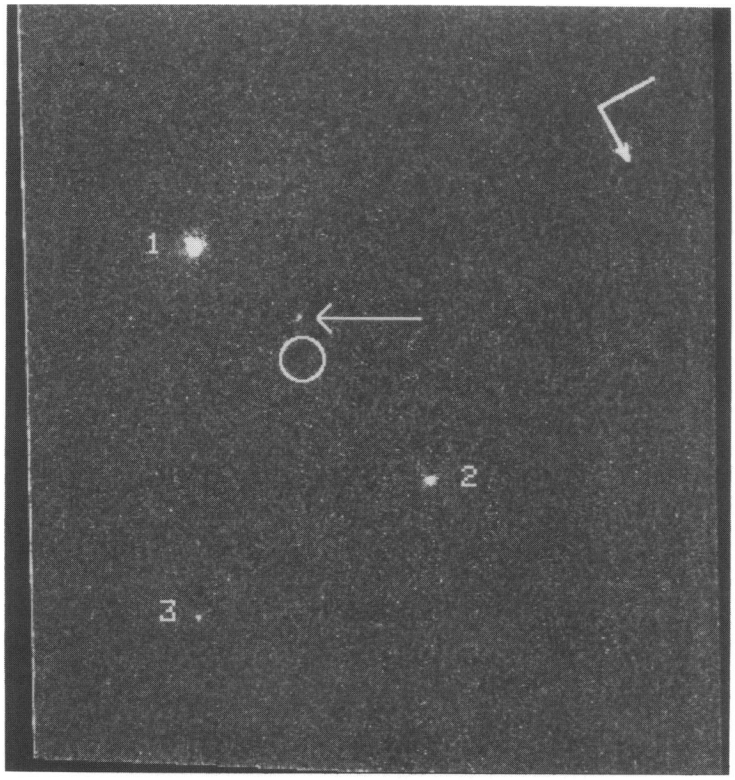

FIG. 3*a*

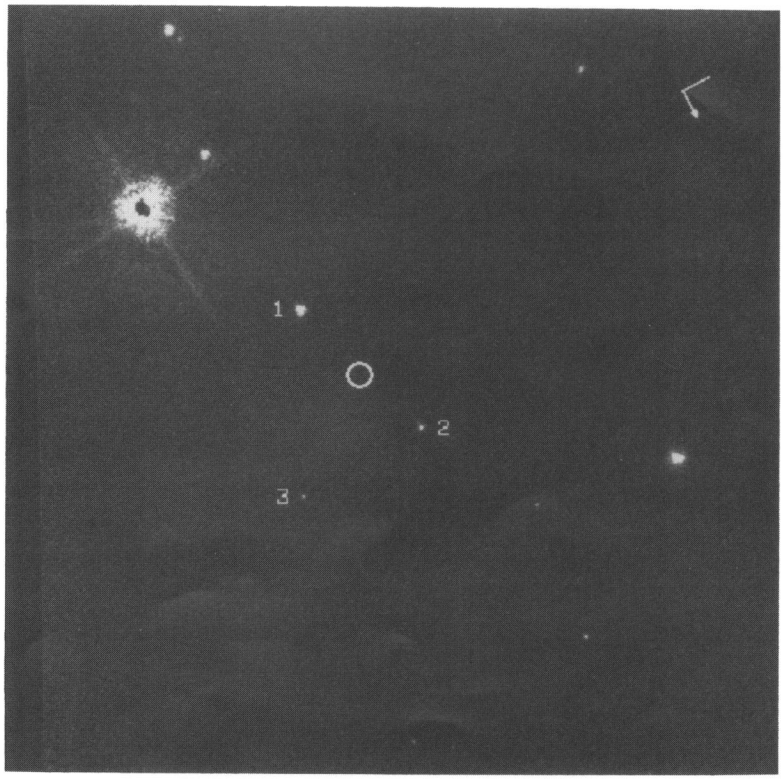

FIG. 3*b*

FIG. 3.—*HST* FOC images for the PSR B1929+10 field in the (*a*) F342W (FOC "U") filter, and (*b*) the F430W (FOC "B") filter. All else is the same as in Plate 1, except the F430W image is in zoomed format with size 14.″7 × 14.″7.

TABLE 3

POSITIONS AND PROPER MOTIONS OF THE RADIO PULSARS

PSR	α_{1950}	δ_{1950}	α_{2000}	δ_{2000}	Epoch	μ_α[a]	μ_δ[a]
B0656+14.....	6 56 57.942 (4)[b]	+14 18 33.80 (2)[b]	6 59 48.134	+14 14 21.31	1993.0[b]	+73(20)[c]	−26(13)[c]
	6 56 57.91 (3)[d]	+14 18 37 (3)[d]	6 59 48.125	+14 14 24.47	1986.2[d]		
			6 59 48.103 (17)[e]	+14 14 19.2 (14)[e]	1991.4[e]		
B0950+08.....			9 53 09.316 (3)[f]	+7 55 35.60 (4)[f]	1985.0[f]	+15(8)[g]	+31(5)[g]
B1929+10.....			19 32 13.874 (6)[h]	+10 59 31.78 (16)[h]	1987.3[h]	+95(15)[h]	+30(20)[h]
			19 32 13.900 (2)[e]	+10 59 31.99 (7)[e]	1991.3[e]		

NOTE—Uncertainties (in parentheses) in the original data refer to the least significant digit quoted. Units of right ascension are hours, minutes, and seconds, and units of declination are degrees, arcminutes, and arcseconds.

[a] Proper motions in milliarcsec yr^{-1}, $\mu_\alpha = \dot{\alpha} \cos \delta$, $\mu_\delta = \dot{\delta}$.

[b] Thompson & Cordova 1994, VLA observations, FK4 coordinates (the aberration E terms are included).

[c] Revised result of Thompson & Cordova 1994.

[d] Dewey et al. 1988, timing observations, the E terms are not included.

[e] Arzoumanian et al. 1994, timing observations.

[f] Fomalont et al. 1992, VLA observations.

[g] Lyne et al. 1982.

[h] Siegman et al. 1994, timing observations.

the use of a poor quality positional calibrator in observations during the first two epochs; the third epoch observations were carried out with a better calibrator. However, this also complicates the evaluation of other potential systematic errors, which may be even larger than 0".2. Comparisons between the timing and interferometric positions of 59 pulsars (Fomalont et al. 1984) shows systematic discrepancies in the range 0".2 – 0".5. A more recent study (Fomalont et al. 1992) showed that nine out of 34 pulsars had discrepancies which exceeded 3 σ. In the same study, comparison between the optical and radio (VLA) positions for the Vela pulsar also showed a discrepancy of about 0".3, indicating that the systematic errors, perhaps originating from the absolute calibration of the optical-radio reference frames (see Fanselow et al. 1984; Ma et al. 1990), are likely to be of this order. The quoted uncertainties of the B0656+14 timing positions are substantially larger than those of the VLA positions (e.g., the declination uncertainties are 3" in Dewey et al. and 1".4 in Arzoumanian et al.). Combined, the timing observations result in the coordinates $\alpha_{2000}(1994.13) = 6^h59^m48^s.126 \pm 0^s.018$ and $\delta_{2000}(1994.13) = 14°14'20".03 \pm 1".30$, compatible with (but less certain than) the VLA coordinates.

B0950+08.— The coordinates of B0950+08 have been reported in many papers during the last few decades (see Fomalont et al. 1984, 1992, and references therein). Earlier measurements are not very useful for our purposes because they were subject to large errors, compounded by uncertainties in the proper motion when the coordinates are transformed to the epoch of the FOC observation (1994.31). The most accurate radio position of this pulsar was determined through VLA observations (epoch 1984.98) by Fomalont et al. (1992). The original FK4 coordinates (B1950; the E terms included) and the J2000 coordinates for the same epoch are presented in Table 4. The proper motion of B0950+08 was determined by Lyne, Anderson, & Salter (1982) and Gwinn et al. (1986); their results are in good agreement. Taking a conservative approach, we use the result of Lyne et al. (1982) for our analysis. It should be noted that an annual parallax of 7.9 ± 0.8 mas was measured for B0950+08 (Gwinn et al. 1986), yielding $d = 127 \pm 13$ pc. Thus, it is one of only a few pulsars with a directly measured distance; most other pulsars have distances determined from the dispersion measure.

B1929+10.—The most recent measurements of the coordinates of B1929+10 have been carried out in timing observations by Siegman, Manchester, & Durdin (1993; epoch 1987.3) and Arzoumanian et al. (1994; epoch 1991.3). When accounting for the pulsar's proper motion (Downes & Reichley 1983; Siegman et al. 1993), these positions are in general agreement, and in accord with previous determinations (e.g., Backer & Sramek 1981, interferometry; Downes & Reichley 1983, timing; Fomalont et al. 1984, VLA). We transformed the coordinates of Siegman et al. and Arzoumanian et al. to the epoch of the FOC observation (1994.52), using the proper motion of Siegman et al., and averaged the results to obtain the expected radio position presented in Table 4. Using the proper motion of Downes & Reichley ($\mu_\alpha = 99 \pm 6$ mas yr^{-1}, $\mu_\delta = 39 \pm 4$ mas yr^{-1}) would lead to practically the same pulsar position at 1994.52. A parallax of 22 ± 8 mas has been reported for this pulsar by Salter, Lyne, & Anderson (1979), which is

TABLE 4

EXPECTED RADIO POSITIONS AND FOC POSITIONS OF THE PULSAR CANDIDATES

		Expected Radio Position[a]		FOC Position[b]		Offsets	
PSR	Epoch	α_{2000}	δ_{2000}	α_{2000}	δ_{2000}	$\Delta_\alpha \cos \delta$	Δ_δ
B0656+14.....	1994.13	6 59 48.139 (6)	14 14 21.28 (3)	6 59 48.093	14 14 21.28	−0.67	0.00
B0950+08.....	1994.31	9 53 09.325 (17)	+7 55 35.89 (18)	9 53 09.210	+7 55 35.22	−1.70	−0.67
B1929+10.....	1994.52	19 32 13.922 (5)	10 59 32.07 (12)	19 32 13.931	+10 59 31.70	+0.13	−0.37

NOTE.—Units of right ascension are hours, minutes, and seconds, and units of declination are degrees, arcminutes, and arcseconds.

[a] Uncertainties do not include systematic errors.

[b] Uncertainties are discussed in the text.

considerably higher than the upper limit of 4 mas determined by Backer & Sramek (1982); the discrepancy has not yet been resolved.

Thus, we have determined the expected radio positions of the three pulsars at the epochs of the FOC observations. The nominal uncertainties attributed to these positions lie in the range 0".08–0".25 for the right ascensions and 0".03–0".18 for the declinations. It should be stressed that these uncertainties do not include possible systematic errors which may be considerably larger, as was discussed for the case of B0656+14.

3.2. *FOC Image Positions*

The expected radio positions for the pulsars listed in Table 4 are designated by the 0".2 circles in Figures 2 and 3. We have used the centroided positions obtained with the APPHOT package routines in IRAF[5] during the photometric analysis (see § 3.3) to measure the coordinates of the pulsar candidates in the FOC images at their observed epochs. A few comments are required to clarify the final FOC positions given in Table 4. To avoid the reseau mark near the image center, the FOC reference position for acquiring B0950+08 was $\simeq$0".5 off the image center. It was discovered after the observations of B0656+14 and B0950+08 that the FOC aperture was misaligned with an error of over 1", and a correction to the FOC aperture position, now including the intentional 0".5 offset from the image center, was implemented on 1994 July 10 (Hack & Nota 1994), in time for our B1929+10 observations. The positions listed in Table 4 for B0656+14 and B0950+08 have been corrected for this misalignment accordingly.

The accuracy of the FOC coordinates is limited by the uncertainties associated with errors of the guide star positions and by the accuracy of the aperture pointing. An aperture verification calibration observation made on 1994 September 4 showed the aperture alignment to be accurate then to within $\sim$0".1 (Hack 1994). Stability of the aperture pointing should be ascertained by future calibration monitoring. The uncertainties of the guide star positions are mainly due to systematic errors (which occur relative to a plate-based coordinate system) of the *HST* Guide Star Catalog (GSC) coordinates (Taff et al. 1990). For the comparison of the radio and FOC positions of our targets, the errors in the *absolute* positions are to be examined; these absolute errors generally exceed the relative errors for pairs of stars. A comparison of the GSC with more precise Carlsberg catalogs showed that the average absolute positional errors from plate center to edge for guide stars of V greater than 10 (the magnitudes of the guide stars used in our observations are V = 10.5–12.8) vary from 0".4 to 0".95 in the northern celestial hemisphere (Taff et al. 1990). Thus, with allowance for both the above-discussed errors of the radio positions and the errors of the FOC positions, we conclude that a typical expected offset for the pulsar counterparts as observed with FOC should be about 0".5–1".5.

The B0656+14 pulsar candidate is offset from its expected radio position by 0".67, well within the total astrometry error budget. While the offset of 1".83 for B0950+08 appears too large, it turns out that the coordinates of the guide stars used to acquire the B0950+08 field have large uncertainties, primarily because they are located near a corner of the Schmidt plate used in their measurement for the GSC. These could be as large as 2" or so (technical assessment rendered by the CAS Branch at STScI). Thus, the object detected also remains a viable pulsar candidate. These are the only candidates for the two pulsars as no other pointlike sources with S/N greater than 3 are detected in these images.

The case for B1929+10 is considerably different, with the field being much more crowded than the others (see Figs. 2*c*, 3*a*, and 3*b*). The measured coordinates of all seven stars detected in the F130LP image are listed in Table 5. There is a small coordinate offset between those measured in the F130LP filter and the other filters of 3–5 pixels ($\sim$0".06), presumably resulting from misalignment of the filter(s) within the optical path of the FOC + COSTAR assemblage. Incorporating various supporting arguments, including color information from our multifilter obser-

[5] IRAF (Image Reduction and Analysis Facility) is distributed by the National Optical Astronomy Observatories, which are operated by the Association of Universities for Research in Astronomy, Inc., under cooperative agreement with the National Science Foundation.

TABLE 5

PHOTOMETRY OF STARS IN 7".4 × 7".4 FIELD AROUND PSR B1929+10

	COORDINATES[a]			F130LP		F342W		F430W			
STAR	R.A. (19 32)	decl. (10 59)	OFFSET	C_{tot} (s^{-1})	$\bar{F}_\nu$[b]	C_{tot} (s^{-1})	$\bar{F}_\nu$[b]	C_{tot}[c] (s^{-1})	$\bar{F}_\nu$[b]	Δm 342W-130LP	Δm 342W-430W ($=m_U - m_B$)
pulsar.....	13.931	31.70	0.39	0.20	6.3	0.052	7.0	(0.074)[d]	<12.	−0.1	<0.6
1	13.894	30.65	1.48	12.33	391.	1.461	197.	5.42	862.	0.7	1.6
2	13.960	33.70	1.72	2.73	87.	0.221	30.	1.20	191.	1.2	2.0
3	13.784	33.80	2.67	1.24	39.	0.057[e]	7.7	0.57	91.	1.8	2.7
4	13.989	29.21	3.03	0.07	2.3	(0.018)[d] [0.016][f]	<2.4 [2.2][f]	(0.074)[d]	<12.	>−0.1	...
5	14.114	33.72	3.27	0.17	5.4	(0.018)[d] [0.039][f]	<2.4 [5.3][f]	(0.070)[d]	<11.	>0.9	...
6	13.967	35.98	3.97	0.14	4.4	(0.018)[d] [0.032][f]	<2.4 [4.3][f]	(0.074)[d]	<12.	>0.7	...

NOTE.—Units of right ascension are hours, minutes, and seconds, and units of declination are degrees, arcminutes, and arcseconds.

[a] Coordinates determined from F130LP images with C24 flat-fielding.

[b] Units of 10^{-31} ergs cm^{-2} s^{-1} Hz^{-1}.

[c] Corrected for zoomed format.

[d] 3 σ upper limits on the total count rate obtained from a circular aperture of 1.7 pixel radius.

[e] Three pixel aperture radius used, instead of standard 6 pixel radius used for the brighter sources.

[f] Count rate and flux expected in F342W filter if $F_\nu \propto \nu^2$.

vations (see below), our best pulsar candidate is shown by the arrow in Figure 2*c*. This is in fact the closest source to the expected radio position with an offset of only 0.″39, the best positional coincidence for any of the three pulsar candidates. The next closest are objects 1 and 2 at 1.″48 and 1.″72, respectively. Detailed examination of the images renders no additional source detections other than those already noted.

One additional piece of astrometric information arises from the $V \approx 13$ star in the upper left corner of the F430W image (Fig. 3*b*). This star is in the *HST* GSC, having coordinates $\alpha_{2000} = 19^h32^m13^s.80$ and $\delta_{2000} = +10°59'27''.4$. The FOC coordinates of this star in our F430W image are $\alpha_{2000} = 19^h32^m13^s.784$ and $\delta_{2000} = +10°59'27''.39$, although we caution that bright objects suffer considerable photometric uncertainties as a result of the limited dynamic range. The core of the bright stellar image is saturated over a significant spatial scale ($\simeq 9 \times 12$ pixels, or $\simeq 0''.15$ radius), and the image point spread function (PSF) is not generally axisymmetric. The difference between the GSC coordinates and the F430W image coordinates is 0.″24 in the right ascension, consistent with both the GSC and FOC measured uncertainties. If we force the FOC coordinates into agreement with the GSC coordinates (assuming the disagreement lies with the *HST* FOC coordinates), the "corrected" coordinates of our pulsar candidate would be $\alpha_{2000} = 19^h32^m12^s.947$ and $\delta = +10°59'31''.71$, and the offset of the candidate from the expected radio position would be $\Delta_\alpha \cos\delta = 0''.37$, $\Delta_\delta = 0''.36$. Although this offset is slightly higher than that in Table 4 (0.″51 vs. 0.″39 for the total angular separation), it is still substantially lower than for other stars in the B1929+10 image.

3.3. *Photometry*

Using the APPHOT package photometry routines in IRAF, we obtained total count rates, C_{tot}, corrected for the background (sky plus detector dark noise) for all objects detected in the F130LP, F342W, and F430W images. The pulsar candidates are listed in Table 2, while the other objects detected in the B1929+10 field are listed in Table 5 along with the B1929+10 candidate. The optimal circular aperture radii (col. [5] in Table 2) used in the final photometry computations were chosen to maximize the S/N ratio of the objects being measured, while upper limits used a radius of 1.7 pixels, corresponding to a sum total of 9 pixels in the aperture. Table 2 also lists the median background (col. [7]) computed in an annulus with a width of 10 pixels at a distance of 20 pixels centered on each object, the source counts corrected for this background (col. [6]), and the measured signal-to-noise ratio (col. [8]). The total source counts (col. [9]) and count rates (col. [10]) include the aperture corrections to the measured counts, for which we have employed the encircled energy tables provided in Version 6.0 of the *HST* FOC Instrument Handbook (Table 8 in Nota, Jedrzejewski, & Hack 1995). For the F130LP and F342W filters, the F346M encircled energy curve was used since its central and pivot wavelengths closely match those of these filters. The F410M encircled energy curve was used for the F430W photometry.

The total count rates have been transformed into mean energy fluxes (see Tables 2 and 5),

$$\bar{F}_\nu = \frac{\int P(\nu) F_\nu \nu^{-1} d\nu}{\int P(\nu) \nu^{-1} d\nu}, \quad (1)$$

using the SYNPHOT package in IRAF. In this definition, $P(\nu)$ is the dimensionless passband throughput function. The advantage underlying the use of such a defined quantity is that for a given count rate the value of $\bar{F}_\nu$ is invariant with respect to the (unknown) spectral shape of the incident flux F_ν.

The count rates and the fluxes presented in Tables 2 and 5 for the F130LP and F342W images have been obtained employing the UV flat field C24 (see § 2). To estimate how the choice of the flat field affects the photometric results, we also analyzed the C1H (blue) flat-field images, along with images that have not been flat-fielded. Note that C24 and C1H bracket both the central and pivot wavelengths of the F130LP and F342W filters. We do not discuss these effects for the F430W image since the pipeline-selected flat field is already a close match. Flat-fielding the B0656+14 image with C24 results in $\lesssim 2\%$ reduction of the background corrected aperture counts for our pulsar candidate, compared with the unflat-fielded image. Using the C1H flat-fielded image results in $\simeq 3\%$ more counts compared to that using C24. There is a larger reduction in the aperture counts for B0950+08, about 10%, in the C24 flat-fielded image than the unflat-fielded image due to its location on the detector, but about the same trend between the C24 and C1H images as noted for B0656+14. The reduction in aperture counts for both the F130LP and F342W images of the B1929+10 candidate are $\simeq 6\%$ in applying the C24 flat field, while an $\simeq 4\%$ increase in aperture counts are seen between using the C1H as opposed to the C24 flat field. Exploration of the aperture counts obtained for the other stars in the B1929+10 field yields changes of $\lesssim 6\%$ in all cases, usually with the same trend as noted previously for the pulsar candidate results. Thus, the overall photometric uncertainties resulting from unknown spectral characteristics of our sources, and consequently in the choice of the appropriate flat field to apply, is $\lesssim 4\%$ for the pulsar candidates.

The comparison of the source fluxes (or upper limits) obtained with the three filters for the B1929+10 field (Table 5) shows that the pulsar candidate identified from the astrometric analysis has a spectrum drastically different from those of the other sources. Although the candidate has not been detected in the F430W image (the profile of a 2.4 σ enhancement at the corresponding position is incompatible with the PSF), even the upper limit indicates that the colors of sources 1–3 are considerably less ultraviolet (see the last column of Table 5). Both the brightness and the high $m_U - m_B$ values ("redness") of these three sources certainly excludes them from the list of pulsar candidates. Further arguments follow from the comparison of the F130LP fluxes with the F342W upper limits for sources 4–6. The F342W band lies approximately in the middle of the wider F130LP band, which means that the spectrum should be either very sharply decreasing (red) or increasing (ultraviolet) with frequency in order to be detected in the F130LP band but not in the F342W band. The fastest expected spectral growth is simply $F_\nu \propto \nu^2$ (a Rayleigh-Jeans spectrum). We calculated the count rates and fluxes which would be produced by this spectrum in the F342W band for the measured F130LP count rates. The results shown in Table 5 (in brackets) demonstrate that the F342W fluxes for sources 5 and 6 substantially exceed the 3 σ upper limits, i.e., the lack of F342W detection means the spectra are also red, and neither can be the pulsar counterpart. Perhaps sources 1–3, 5, and 6 are all very distant white

dwarfs strongly reddened by interstellar extinction. For source 4, which is very faint, the expected F342W flux is close to the 3 σ limit, so we cannot exclude it based on photometry alone. However, its positional offset of 3".03 renders it a very unlikely candidate for B1929+10. Thus, considering *both* the astrometric and photometric analysis, the best candidate for the pulsar B1929+10 is the one marked by an arrow in Figure 2*c*.

Besides the firmly detected pointlike sources, there are numerous local enhancements most of which can certainly be attributed to statistical noise in the images, or to filter/detector blemishes.

In the B0656+14 image we found five local enhancements at $\simeq 2.8\ \sigma$, located at the pixel coordinates [122, 196], [128, 315], [153, 214], [356, 34], and [365, 131]. The 3 σ upper limit corresponds to about 85 *total* counts ($\simeq 35$ counts in the aperture of 1.7 pixel radius chosen to obtain the optimal S/N ratio for the faintest sources), which is 54 times fainter than the proposed pulsar candidate.

The B0950+08 image has about the same background level as B0656+14. Four enhancements were found: [133, 96] at 2.7 σ, [152, 208] at 2.9 σ, [277, 78] at 3.0 σ, and [364, 247] at 3.4 σ. Examination of the individual F130LP images showed the latter two to be false detections, resulting from the sum of fortuitously placed single pixel enhancements in the summed image, with improperly behaved PSFs. The former two enhancements remain inconclusive just below the 3 σ level. Finally, for B1929+10, no excesses at levels $\geq 2.7\ \sigma$ were found in the F130LP image, which has a 3 σ background level of 51 total counts, a factor of 4.8 fainter than our pulsar candidate. Three enhancements were found in the summed F342W image, which has a 3 σ background level of 61 total counts: [98, 303] at 3.1 σ, [136, 388] at 2.7 σ, and [142, 153] at 2.9 σ. Examination of the individual F342W images revealed significant enhancements in one of the images at roughly the S/N noted, but not in the other image. Furthermore, none of these are seen in the F130LP image. Thus, these again appear to be false pseudodetections.

3.4. *Interpretation*

3.4.1. *B0656+14*

The mean flux $\bar{F}_\nu = (3.05 \pm 0.15) \times 10^{-30}$ ergs cm^{-2} s^{-1} Hz^{-1} = (0.305 ± 0.015) μJy in the F130LP filter is shown as a wide cross in Figure 4. In estimating the associated uncertainty we have included contributions from both the counting statistics ($\simeq 2\%$) and a possible systematic error in the flat-fielding ($\simeq 3\%$; see §§ 2 and 3.3). The horizontal error bar shows the FWHM of the filter throughput, $\lambda\lambda = 2310$–4530 Å, centered at the pivot wavelength 3365 Å. The corresponding (isotropic) luminosity of the source in this band is $L_\infty^{(130LP)} \simeq 4\pi d^2 \bar{F}_\nu \Delta\nu \simeq 5.8 \times 10^{28} d_{500}^2$ ergs s^{-1}, where $d_{500} = d/500$ pc. The distance d is, in fact, poorly known (see Table 1); the dispersion-measure–based distance was estimated as 760 pc, with an uncertainty of ~ 200 pc (Taylor, Manchester, & Lyne 1993), but the *ROSAT* data suggest a lower distance, in the range ~ 200–500 pc (Córdova et al. 1989; Finley, Ögelman, & Kiziloğlu 1992; Anderson et al. 1993). Thus, the F130LP luminosity may lie within the wide range $L_\infty^{(130LP)} = (0.5$–$20) \times 10^{28}$ ergs s^{-1}, or $(0.1$–$5) \times 10^{-6}$ of the spin-down luminosity $\dot{E}$.

Since our original goal was to detect the thermal-like radiation from the NS surface, we used the *ROSAT* PSPC data (~ 6500 photons in 3200 s; Finley et al. 1992) to extrapolate the soft X-ray spectral flux (attributable to the NS surface radiation) to the UV-optical range. The result of this extrapolation depends on the model assumed to fit the soft X-ray spectrum. The blackbody fit of the *ROSAT* spectrum yields $T_\infty^{bb} = (9.0 \pm 0.4) \times 10^5$ K for the redshifted temperature measured by a distant observer, and $d = 500$ pc for the distance if the apparent NS radius is assumed to be $R_\infty = 10$ km (Finley et al. 1992).

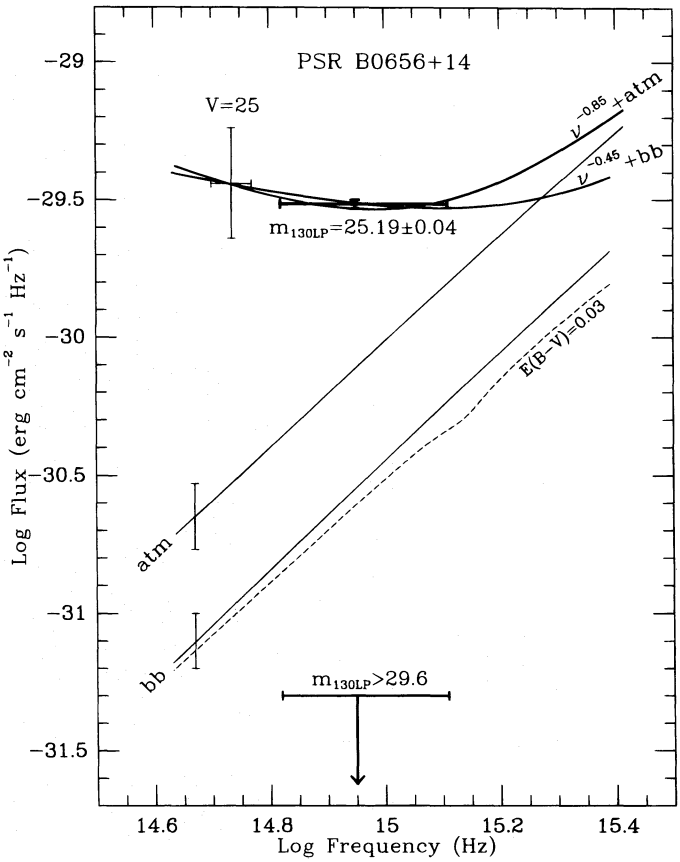

FIG. 4.—The wide cross shows the energy flux detected from the PSR B0656+14 candidate with the F130LP filter (m_{130LP} is the stellar AB magnitude). The 3 σ upper limit on the flux from undetected sources is shown at the bottom of the figure, along with the corresponding AB magnitude. The cross labeled "$V = 25$" shows the result by Caraveo et al. (1994b) obtained from ground-based observations. The lines labeled "bb" and "atm" are obtained by fitting the thermal soft X-ray *ROSAT* spectrum with different models: the "bb" line represents the blackbody model, and the "atm" line corresponds to a magnetic model atmosphere (Pavlov et al. 1995). The vertical bars at these lines illustrate uncertainties of the model fits. The dashed line illustrates the difference between the attenuated and nonattenuated "bb" spectra for a reasonable value of the interstellar extinction. Best fits of the data with two-component models, combining a power law with either a "bb" or an "atm" model, are shown by the thick lines. The spectra are shown in the range $\lambda\lambda \simeq 1200$–$7000$ Å observable with *HST*.

Instead of the simplistic blackbody model, one can fit the soft X-ray spectrum with a set of magnetic NS atmosphere models (Pavlov et al. 1995). Such a fit with values of the magnetic field strength $B = 4.7 \times 10^{12}$ G, mass $M = 1.4\ M_\odot$, and radius $R_\infty = 13$ km ("true" radius being $R = 10$ km) gives the atmospheric model effective temperature $T_\infty^{eff} = 5.3^{+0.4}_{-0.5} \times 10^5$ K and $d = 280^{+60}_{-50}$ pc (Anderson et al.

1993).[6] The atmosphere model spectrum at $h\nu \ll kT$ is the sum of two fluxes with orthogonal (ordinary and extraordinary) polarizations. The flux in the ordinary mode follows the Rayleigh-Jeans law, $F_\nu \simeq 0.5 B_\nu(T_s)$ at the NS surface, with a surface temperature $T_s < T^{\rm eff}$ ($T_s \simeq 0.42 T^{\rm eff}$ for the specific model considered). The extraordinary flux originates from deeper layers, where the temperature is close to (or slightly exceeds) $T^{\rm eff}$; its shape only slightly differs from that of the Rayleigh-Jeans spectrum in the narrow UV-optical range. The best fitting model total (ordinary + extraordinary) flux extended down into the UV-optical is labeled as "atm" in Figure 4. The atmosphere model flux is higher than that of a blackbody because the best-fitting distance is closer. Nevertheless, the predicted model flux in the F130LP bandpass from the fit to the *ROSAT* data still falls a factor of 4 lower than the F130LP flux of our pulsar candidate.

Hence, if this, the only firmly detected pointlike source in the image, is indeed the pulsar counterpart, its radiation should be predominantly of a *nonthermal origin*. On the other hand, if we assume that this is not the pulsar, the 3 σ limit on the point-source flux, $\bar{F}_\nu < 5 \times 10^{-32}$ ergs cm^{-2} s^{-1} Hz^{-1}, also shown in Figure 4, is considerably lower than the flux predicted by either blackbody or magnetic atmosphere models. The flux limit corresponds to the following limitation on the (blackbody) temperature of the NS surface: $T_\infty^{\rm bb} < 1.0 \times 10^5 d_{500}^2 R_{13}^{-2}$ K, where $R_{13} = R_\infty/13$ km. This low limiting temperature certainly disagrees with the *ROSAT* data, providing strong evidence that *the star we detected is indeed the pulsar counterpart*. Moreover, this temperature is considerably lower than predicted by most NS cooling models given an age of $\simeq 10^5$ yr (e.g., Van Riper 1991), unless its distance is much greater than 500 pc.

Also plotted is an ~ 3 σ ground-based V detection of a source in the field of B0656+14 (Caraveo et al. 1994a). Assuming this is a true detection (but with large uncertainties), this must be the same star we detected (with a considerably deeper exposure) in the F130LP band. If further observations confirm this V detection, it would support our conclusion about the nonthermal nature of the UV-optical spectrum: the V and F130LP fluxes cannot be simultaneously fitted with a (Rayleigh-Jeans tail) thermal spectrum.

To separate the nonthermal component and to estimate the slope of its spectrum, we assumed the nonthermal spectrum to be a power law and fitted the two spectral points, the F130LP and V fluxes, with the sum $F_\nu = F_\nu^{\rm th} + F_\nu^0 (\nu/\nu_0)^{-\alpha}$, where $F_\nu^{\rm th}$ is either "bb" or "atm" thermal model spectrum, $\nu_0 = 5.43 \times 10^{14}$ Hz is the central frequency of the V filter, and α and F_ν^0 are the fitting parameters. The best fits for $V = 25$ ($\alpha = 0.45$, $F_\nu^0 = 3.5 \times 10^{-30}$ for "bb", and $\alpha = 0.85$, $F_\nu^0 = 3.3 \times 10^{-30}$ for "atm") are shown in Figure 4. For the range $24.5 < V < 25.5$, the fit gives $-0.4 < \alpha < 1.5$ and $-0.2 < \alpha < 1.9$ for the "bb" and "atm" thermal models, respectively. These results predict that we should expect a rise of the flux in the far-UV domain, observable with *HST*, and this rise is different for the two models of thermal radiation (see Fig. 4).

[6] A similar best-fit temperature (with much greater uncertainties) has been reported recently by Foster, Edelstein, & Bowyer (1996) based on *EUVE* DS (Deep Survey instrument) detection of B0656+14. Note that the flux detected by the *EUVE* DS is apparently dominated by soft X-rays ~ 0.1 keV.

An additional restriction on the slope of the nonthermal component can be obtained by extending the UV-optical power law into the *ROSAT* band. Since the soft part of the PSPC spectrum (at $E \lesssim 1$ keV) looks certainly thermal-like, we should require that the power-law component be lower than the observed X-ray flux at $0.1 \lesssim E \lesssim 1$ keV. This yields $\alpha \gtrsim 0.2$, which is compatible with the UV and optical fluxes. It is interesting to note that a subsequent 13 ks *ROSAT* PSPC observation of B0656+14 found a faint hard component ($E \gtrsim 1$ keV) of the X-ray spectrum (Finley 1994). This could be the high-energy extension of our nonthermal UV-optical radiation, provided the power-law index $\alpha \sim 0.3$. Otherwise, at higher α, the hard X-ray component is either thermal radiation from a hot polar cap or nonthermal radiation of a different origin.

In the above analysis we neglected interstellar extinction of the UV-optical radiation. The total extinction at a given wavelength, A_λ, can be evaluated for a given color excess $E(B-V)$ assuming the extinction curve toward the object is known. From the compilation presented by Fruscione et al. (1994), the closest stars toward B0656+14 ($l = 201\overset{\circ}{.}1$, $b = 8\overset{\circ}{.}3$, $d = 200$–700 pc) yield $E(B-V)$ values of 0.04 ($l = 204\overset{\circ}{.}7$, $b = 2\overset{\circ}{.}8$, $d = 347$ pc), 0.07 ($l = 202\overset{\circ}{.}9$, $b = 2\overset{\circ}{.}2$, $d = 692$ pc), 0.01 ($l = 195\overset{\circ}{.}8$, $b = -2\overset{\circ}{.}1$, $d = 169$ pc), and 0.01 ($l = 196\overset{\circ}{.}5$, $b = -1\overset{\circ}{.}6$, $d = 755$ pc). All these stars have lower latitudes and presumably higher extinction than B0656+14. The nearest stars at latitudes higher than B0656+14 are too distant to render any definitive conclusion on $E(B-V)$. Rough extrapolations to closer distances give $E(B-V) \lesssim 0.01$–0.02. Another method of estimating the extinction uses the hydrogen column density found from UV or X-ray observations. Savage & Mathis (1979) suggest the following relation: $E(B-V) \simeq n_{\rm H}/(5.8 \times 10^{21}$ cm$^{-2})$. Finley et al. (1992) obtain $n_{\rm H} = (1.0 \pm 0.2) \times 10^{20}$ cm^{-2} from their blackbody fit to the *ROSAT* spectrum of B0656+14, which gives $E(B-V) \simeq 0.02$, in agreement with our estimates from the color excesses of nearby stars. An even smaller value of $n_{\rm H}$ was obtained when fitting the *ROSAT* spectrum with an NS atmosphere model (Anderson et al. 1993): $n_{\rm H} = (0.5 \pm 0.2) \times 10^{20}$ cm^{-2}, which corresponds to $E(B-V) \simeq 0.01$. Thus, a reasonable range is $E(B-V) = 0.01$–0.03, but certainly less than 0.07. Taking a reasonably large value of $E(B-V) = 0.03$ corresponds to $A_V = 0.09$ mag (Savage & Mathis 1979). Even at the UV bump (2190 Å) where the maximum total extinction occurs, it only amounts to 0.24 mag, and the corresponding attenuation of the spectral flux is 25%. Such attenuation has little impact on our previous conclusions; its inclusion only slightly reduces the contribution of the thermal component to the observed UV-optical fluxes (see Fig. 4).

3.4.2. *B0950+08*

The flux of the only firmly detected pointlike source in the B0950+08 image is $\bar{F}_\nu = (5.1 \pm 0.3) \times 10^{-31}$ ergs cm^{-2} s^{-1} Hz^{-1}, about 6 times fainter than that of B0656+14. If this object is the pulsar, its luminosity in the F130LP band is $L_\infty^{(130{\rm LP})} \simeq 7 \times 10^{26} d_{130}^2$ ergs s^{-1} $\simeq 1.2 \times 10^{-6} d_{130}^2 \dot{E}$.

B0950+08 was observed with the *ROSAT* PSPC, although only 55 source counts were detected in $\simeq 9$ ks (Manning & Willmore 1994), too few to draw any firm conclusions about the shape and origin of the soft X-ray spectrum. It is not even clear whether this radiation is produced by the pulsar itself or by an unresolved compact nebula. Manning & Willmore fitted both blackbody and

power-law models to the observed counts. Their best fit for the blackbody gave $T_\infty^{bb} = 2.1 \times 10^6$ K and a radius for the emitting region of only $r \lesssim 20$ m. Such radiation could originate from a hot polar cap. Extending their blackbody fit into the UV-optical range gives $F_\nu \simeq 5.3 \times 10^{-35}(\nu/8.9 \times 10^{14}\ \mathrm{Hz})^2$ ergs cm^{-2} s^{-1} Hz^{-1} for the flux at the pivot wavelength of the F130LP band, 4 orders of magnitude lower than what we observed. Thus, if the radiation observed with *ROSAT* is indeed thermal radiation from the hot spot, it is much too faint to be detected in the UV-optical range, and the radiation we detected must be produced in some other fashion, presuming that our candidate is indeed the pulsar.

Assuming our F130LP flux is thermal in origin, but arises instead from the *entire* NS surface, the resulting blackbody fit to this flux gives $T_\infty^{bb} = (7.0 \pm 0.4) \times 10^4$ K for $d = 130$ pc and $R_\infty = 13$ km (the latter value corresponds to the "canonical" NS mass 1.4 $M_\odot$ and radius $R = 10$ km; notice that the temperature as measured at the NS surface would be a factor $1 + z = [1 - (2GM/Rc^2)]^{-1/2} \simeq 1.3$ higher). This spectral blackbody fit is shown in Figure 5. The corresponding bolometric luminosity is $L_\infty^{bol} = (2.9 \pm 0.7) \times 10^{28}$ ergs s^{-1}. Considering the uncertainties on d ($\sim$10%) and R ($\sim$30%), the allowable temperature and bolometric luminosity ranges are $(7 \pm 4) \times 10^4$ K and (0.15–32) $\times 10^{28}$ ergs s^{-1}. The actual T_∞^{eff} of the NS atmosphere model might be slightly higher because of radiative transfer effects in the presence of strong magnetic fields. (Although NS atmosphere models cannot be constructed at this time for temperatures this low, we anticipate no more than about a 10% difference to occur). Extrapolating this fit into the *ROSAT* band (0.08–2.4 keV) gives a luminosity at least an order of magnitude lower than the value obtained by Manning & Willmore ($\simeq 8 \times 10^{28}$ ergs s^{-1} for $d = 130$ pc). This is not surprising because, for the temperatures inferred, the peak of the spectral flux lies in the far-UV or EUV domains, at energies much lower than the *ROSAT* bandpass. Thus, the assumption that we detected thermal radiation from the NS surface does not conflict with the information provided by the *ROSAT* data.

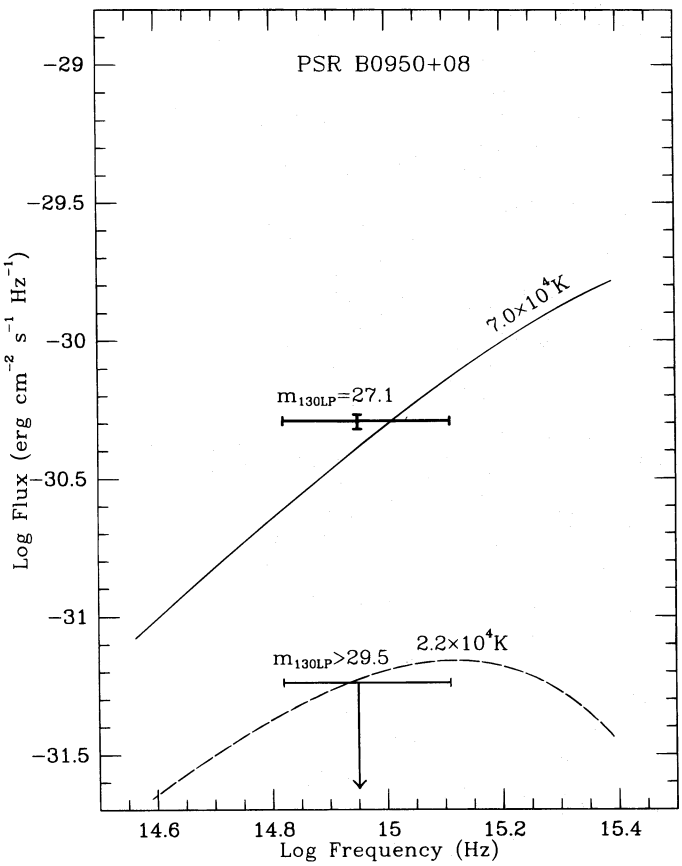

FIG. 5.—Flux observed from the PSR B0950+08 candidate in the F130LP filter and the 3 σ upper limit on the flux of undetected sources are displayed. The curves show best-fit blackbody spectra for the observed flux (*solid*) and the upper limit (*dashed*), for the distance $d = 127$ pc and the NS radius $R_\infty = 13$ km, labeled with the corresponding temperatures T_∞^{bb}.

The 3 σ upper limit on the F130LP flux from an undetected source is $\bar{F}_\nu \simeq 5.5 \times 10^{-32}$ ergs cm^{-2} s^{-1} Hz^{-1}. Interpreted as a blackbody flux, it corresponds to the NS surface temperature $T_\infty^{bb} = 2.2 \times 10^4$ K at $d = 130$ pc, $R_\infty = 13$ km (see Fig. 5), an extremely low temperature even for such an old pulsar as B0950+08 (see § 4).

The power-law model fits obtained by Manning & Willmore have very broad 90% confidence limits on the index of $-0.2 < \alpha < 3.1$, with the best-fit value $\alpha = 0.9$. Such a model only matches our F130LP flux if the index lies within the range $\alpha \simeq 0.26$–0.35, whereas the best-fit α gives an unacceptably high UV flux of $F_\nu \simeq 10^{-29}$ ergs cm^{-2} cm^{-1} Hz^{-1} at the pivot wavelength. The *ROSAT* data have very poor statistics, so one cannot completely exclude the possibility that both the UV-optical and soft X-ray fluxes are produced via nonthermal processes. However, in this case the UV efficiency, $\eta = L_{130LP}/\dot{E}$, of this very old pulsar would be improbably high, comparable to the much younger B0656+14. Therefore, we consider this possibility much less plausible.

As B0950+08 is both closer and located at a higher Galactic latitude than B0656+14, the interstellar extinction is expected to be even less important than for B0656+14. Manning & Willmore (1994) obtained a 90% upper limit on n_H of 1.8×10^{20} cm^{-2}, and the actual value is likely less than 10^{20} cm^{-2}, which corresponds to $E(B-V) \lesssim 0.02$. The closest stars in the compilation of Fruscione et al. (1994) lie $\sim 20°$ apart from B0950+08 and show no measurable extinction at all; n_H in this vicinity does not exceed 1×10^{20} cm^{-2}. Neutral hydrogen 21 cm absorption measurements provide an even smaller limit on n_H than that above (Dickey et al. 1981). This level of interstellar extinction is entirely negligible for our present analysis, so we forgo any further discussion of extincted models for B0950+08.

3.4.3. *B1929+10*

As we concluded from the astrometric and photometric analysis in §§ 3.1 and 3.2, there is only one plausible pulsar candidate among seven stars detected in the 7.″4 × 7.″4 B1929+10 field. Interpretations of the observed radiation depend on the distance to the pulsar and the interstellar extinction which, unfortunately, are rather uncertain. The parallax measurements of Salter et al. (1979) yield $d = 30$–80 pc, whereas the upper limit on the parallax obtained by Backer & Sramek (1982) corresponds to $d > 250$ pc (see § 3.1). For the reference distance we adopt the value $d = 170$ pc determined by Taylor et al. (1993) from the radio dispersion measure.

The results on $E(B-V)$ and n_H (Fruscione et al. 1994) obtained from direct measurements of stars close to B1929+10 ($l = 47.^\circ4$, $b = -3.^\circ9$) are somewhat controversial. The two closest stars show quite different values:

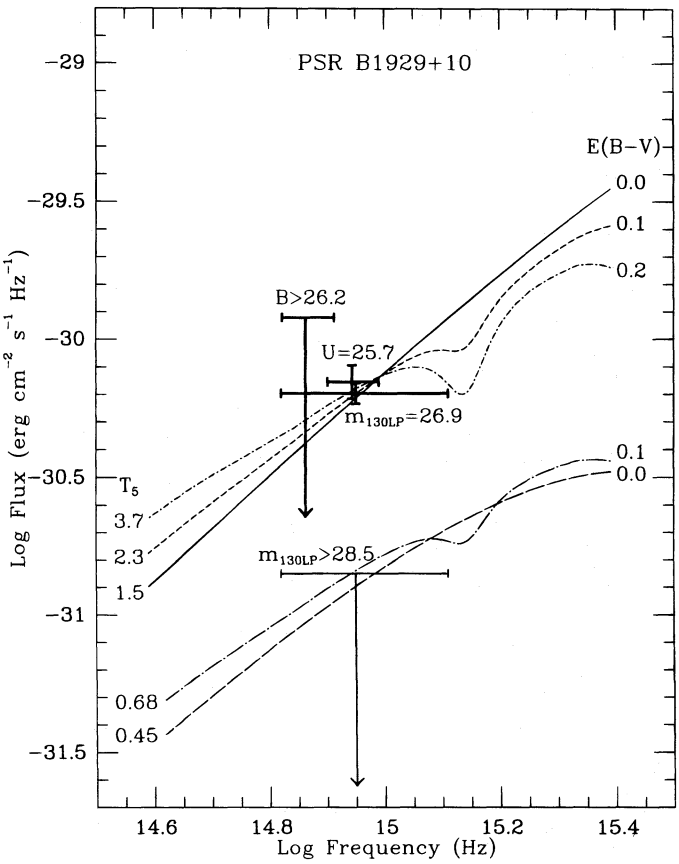

FIG. 6.—Fluxes observed from the PSR 1929+10 candidate in the F130LP and F342W filters and the 3 σ upper limit in the F430W filter are displayed. The 3 σ upper limit on the flux from undetected objects in F130LP is shown at the bottom. The U and B magnitudes of the pulsar candidate are presented in the standard Vega magnitudes. The corresponding AB magnitudes are $m_U = 26.8$ and $m_B > 26.2$. The solid, short-dashed, and short dot-dashed curves show best-fit blackbody spectra to the fluxes observed for the interstellar extinctions $E(B-V) = 0.0$, 0.1, and 0.2, respectively. The long-dashed and long dot-dashed curves show the best fits to the upper limit for $E(B-V) = 0.0$ and 0.1. The corresponding temperatures $T_5 = T_\infty^{bb}/(10^5$ K), for $d = 170$ pc and $R_\infty = 13$ km, are depicted near the curves.

log $n_H < 19.0$, $E(B-V) = 0$ for WD 1936+047 ($l = 39\overset{\circ}{.}7$, $b = -2\overset{\circ}{.}5$, $d = 210$ pc) and log $n_H = 21.0$, $E(B-V) = 0.23$ for σ Aql ($l = 43\overset{\circ}{.}3$, $b = -8\overset{\circ}{.}1$, $d = 140$ pc). The other five nearby stars show log $n_H < 19.7$ and no measurable extinction, except 66 Oph ($l = 31\overset{\circ}{.}0$, $b = 13\overset{\circ}{.}4$) for which log $n_H = 20.8$ and $E(B-V) = 0.19$. This suggests that the ISM is very patchy in that direction, and the radio and soft X-ray data obtained directly from B1929+10 would be more reliable. The 21 cm observations of B1929+10 by Weisberg, Rankin, & Boriakoff (1980) give $n_H \simeq (1\text{–}2) \times 10^{20}$ cm^{-2}, which corresponds to $E(B-V) \simeq 0.02\text{–}0.04$. The values of n_H obtained from fits to the *ROSAT* spectrum of this object show large variations (see below) ranging from $\sim 10^{19}$ to $\sim 10^{21}$ cm^{-2}, with a typical value $\simeq (1\text{–}2) \times 10^{20}$ cm^{-2} consistent with the 21 cm observations. Thus, we adopt $E(B-V) = 0.02\text{–}0.04$ as a likely range, 0.1 as a plausible upper limit, and 0.2 as a very conservative upper limit. With the adopted $E(B-V)$ values, the (unabsorbed) luminosity in the F130LP band can be estimated as $L_\infty^{(130LP)} \simeq (1\text{–}3) \times 10^{27} d_{170}^2$ ergs s^{-1} $= (3\text{–}8) \times 10^{-7} d_{170}^2 \dot{E}$.

Although the pulsar candidate was detected with two spectral filters, and an upper limit was established in the F430W filter, these results alone do not allow one to make very definite conclusions about its spectrum: the F342W spectral band lies in the middle of the F130LP band, and the F430W exposure was too short. Fitting the fluxes in the two bands with the blackbody and power-law models puts rather broad limits on the spectral temperature and power-law index, excluding only very sharply rising or falling spectra. If, for instance, we neglect extinction and choose a spectral parameter and a normalization factor which gives a best fit in one of these bands, then the count rate lies within ± 1 σ from the count rate detected with the other filter in the parameter space $6100 < T < 32{,}000$ K and $-0.7 < \alpha < 2.5$. If we fit the flux in one of the filters with the Rayleigh-Jeans spectrum, the count rate in the other filter differs by 2.3 σ from the measured one. The difference decreases [down to 1.7 σ at $E(B-V) = 0.1$, and 1.1 σ at $E(B-V) = 0.2$], and the 1 σ temperature and power-law domains shift when the extinction is applied to the spectrum: $6400 < T < 55{,}000$ K, $-1.3 < \alpha < 2.2$ for $E(B-V) = 0.1$, and $6800 < T < 300{,}000$ K, $-1.9 < \alpha < 2.0$ for $E(B-V) = 0.2$. This means, in particular, that one at least cannot exclude that the radiation detected is predominantly thermal, and the corresponding temperature is sufficiently high to be attributed to the NS surface.

Some restrictions on the nature of the UV-optical radiation can be obtained from comparison with the soft X-ray observations of the pulsar. Yancopoulos, Hamilton, & Helfand (1994) report on *ROSAT* PSPC observations of B1929+10: $\simeq$420 photons in the 0.1–2.0 keV band were detected in 45 ks. From their analysis, the blackbody fit of the spectrum yields $T_\infty^{bb} \simeq 3.2 \times 10^6$ K, a radius for the emitting region of $\lesssim 30(d/250\text{pc})$ m, and $n_H \simeq 1.3 \times 10^{20}$ cm^{-2}. Similar to B0950+08, the radiation is attributable to a hot polar cap. Fitting the same spectrum with a set of magnetic atmosphere models at $B = 1.2 \times 10^{12}$ G gives a lower effective temperature $T_\infty^{eff} = 2.2^{+0.6}_{-0.4} \times 10^6$ K, higher hydrogen column density $n_H = 1.9^{+2.1}_{-1.1} \times 10^{20}$ cm^{-2}, and a few times larger radius of the emitting region (Meyer & Pavlov 1993). Extending both the blackbody and atmosphere model spectra for the hot polar cap into the UV-optical range yields a very low flux, $F_\nu < 10^{-34}$ ergs cm^{-2} s^{-1} Hz^{-1} at $\lambda = 3400$ Å, which cannot account for the radiation we detected. Fitting the *ROSAT* spectrum with the power-law model gives $\alpha = 1.0 \pm 0.4$ and $n_H = 6.5^{+3.5}_{-2.1} \times 10^{21}$ cm^{-2} (Meyer & Pavlov 1993). Extending this into the range of our *HST* observations, we obtain a much higher flux than observed, $F_\nu \sim (0.03\text{–}10) \times 10^{-28}$ ergs cm^{-2} s^{-1} Hz^{-1} at $\lambda = 3400$ Å; the observed UV flux can be matched with the *ROSAT* flux only if $\alpha \simeq 0.05\text{–}0.15$, which is excluded by the X-ray fit with a probability greater than 99%. Thus, the UV-optical radiation we detected is of a different nature than either the thermal (hot polar cap) or power-law interpretations of the *ROSAT* spectrum.

The PSPC spectrum does not exclude a faint soft component in addition to the dominating "hard component;" the former may originate from the entire NS surface with a temperature lower than that of the polar cap. Yancopoulos et al. (1994) analyzed the count spectrum at $E < 0.3$ keV and estimated an upper limit on the global (blackbody) surface temperature of 2.7×10^5 K, for $R_\infty = 10$ km, $d = 250$ pc, and $n_H = 1.5 \times 10^{20}$ cm^{-2}. This corresponds, for the same values of R_∞, d, and n_H, to the UV flux $F_\nu < 3 \times 10^{-31} (\nu/9 \times 10^{14}$ Hz$)^2$ ergs cm^{-2} s^{-1} Hz^{-1}, about a factor of 2 lower than the flux detected in the F130LP and F342W bands. Fitting the whole PSPC spectrum with two-

component (hard + soft) models carried out by Meyer & Pavlov (1993) shows that the upper limits on the effective surface temperature strongly depend on the range of allowed distances and hydrogen column densities assumed, as well as on the specific model spectra chosen for fitting. Various fits yield, at the 99% confidence level, the limits in the range (1–4) $\times 10^5$ K. If we assume that the UV flux we observed is the thermal radiation originating from the entire NS surface, then we can choose realistic R and d to infer a temperature within the above limits which fits our results. For instance, if $R_\infty = 13$ km and $d = 170$ pc, then the best-fit blackbody temperature (for zero extinction) is $T_\infty^{bb} = 1.5 \times 10^5$ K (see Fig. 6). If the true $E(B-V)$ value is higher, the UV flux might be substantially attenuated, and the observed flux would correspond to a temperature higher than that for $E(B-V) = 0$. In Figure 6 the best-fit attenuated fluxes are shown for $E(B-V) = 0.1$ and 0.2 which correspond to the temperatures 2.3 and 3.7×10^5 K. For the most plausible range of $0.02 < E(B-V) < 0.04$, the temperatures consistent with the fluxes detected are $T_\infty^{bb} = (1.4\text{–}2.1) \times 10^5$ K. If we allow a wider range for the extinction, $E(B-V) = 0.0\text{–}0.1$, then the range of the blackbody temperatures for the same $d = 170$ pc and $R_\infty = 13$ km is $T_\infty^{bb} = (1.3\text{–}2.7) \times 10^5$ K. For larger d and/or smaller R_∞ the temperatures would increase; e.g., for $d = 250$ pc and $R_\infty = 13$ km they would be $\sim(3\text{–}6) \times 10^5$ K. The latter temperatures seem too high for this relatively old pulsar, which may mean that either the true distance is smaller or the radiation we observed is a combination of thermal and nonthermal components. To verify this and separate the components, additional observations with more filters are required.

Finally, if we accept the (unlikely) assumption that both the proximity to the radio pulsar position and the difference of the spectrum from those of the field stars are due entirely to chance then the 3 σ limit on the temperature of the undetected pulsar would be $T_\infty^{bb} < (4\text{–}7) \times 10^4$ K for $d = 170$ pc and $0 < E(B-V) < 0.1$ (see Fig. 6).

4. DISCUSSION

Based on the above astrometric and photometric analysis, together with results from *ROSAT* observations, we believe that we have detected the UV-optical counterparts of all the three pulsars. To firmly reject the hypothesis of accidental coincidence, further observations (timing, multicolor photometry, astrometry, polarimetry) would be needed. Until such observations are carried out, the possibility that the counterparts are fainter than the faint limits imposed by our observations cannot be completely excluded (although we consider this very unlikely, at least for B0656+14 and B1929+10). Thus, the results of our observations and analysis can be summarized as follows.

1. If the objects we detected are indeed the UV-optical pulsar counterparts, then:

a) The radiation of B0656+14 is predominantly nonthermal in the optical through near-UV range. The thermal component emitted by the NS surface should become dominant in the far-UV domain, and would be observable with *HST*. Adopting the estimate of the pulsar V magnitude by Caraveo et al. (1994a), the nonthermal spectrum can be approximated by a power law, $F_\nu \propto \nu^{-\alpha}$, with the index $-0.4 \lesssim \alpha \lesssim +1.9$. If the power law has the same slope up to the soft X-ray energy range, the index should be $\gtrsim 0.2$.

b) The radiation of B1929+10 is either thermal or is an admixture which includes a nonthermal component, depending on the distance and interstellar extinction adopted. If the radiation is purely thermal, the mean temperature over the NS surface is $T_\infty^{bb} = (1\text{–}3) \times 10^5$ K (for $d = 150\text{–}200$ pc, $R_\infty = 13$ km, and $E(B-V) = 0.02\text{–}0.04$). If a nonthermal component contributes (which can be verified by additional observations with more filters), the temperatures above represent upper limits.

c) The presence of a perceptible nonthermal component in the radiation of B0950+08 looks very implausible. Its thermal radiation can be produced by the NS surface with a temperature $T_\infty^{bb} = (7 \pm 1) \times 10^4$ K (for $d = 127 \pm 13$ pc and $R_\infty = 13$ km).

2. If the pulsars are too faint in the UV-optical to have been detected, even with our extremely deep exposures, we can then place very low upper limits on the NS surface temperatures: $T_\infty^{bb} < 1.0 \times 10^5$ K for B0656+14 at $d = 500$ pc; $T_\infty^{bb} < 7 \times 10^4$ K for B1929+10 at $d = 170$ pc; and $T_\infty^{bb} < 2.2 \times 10^4$ K for B0950+08 at $d = 130$ pc (all the estimates are for $R_\infty = 13$ km).

We discuss briefly some implications of these results.

Conclusion (1*a*) about the nonthermal origin of the optical flux from B0656+14, as well as the possible presence of a nonthermal component in the radiation detected from B1929+10, is in severe disagreement with the simple model of Pacini (1971):[7] $L_{opt} \propto B^4 P^{-n} \Delta r$, where B is the magnetic field strength at the pulsar surface, P is the period, Δr is the radial extension of the emitting region, and n has a value $\sim$8–10, depending on assumptions pertaining to the energy spectrum of synchrotron-radiating electrons.

This model describes fairly well the relation between the optical luminosities of the Crab and Vela pulsars ($n \simeq 10$), but fails to account for the optical pulses observed from B0540−69 in the LMC (Middleditch & Pennypacker 1985); the corresponding value of n would be 2.4 and 1.5 if compared with the Crab and Vela pulsars. A modification of the original model was suggested (Pacini & Salvati 1987) to allow for different duty cycles of pulsars, pitch angles of radiating electrons, and power-law indices of the observed nonthermal radiation. When applied to B0656+14, with the Crab pulsar as a reference source, this modified model predicts an optical luminosity $\sim 10^{23}$ ergs s^{-1}, which is at least 5 orders of magnitude lower than observed and 3 orders of magnitude below the lower limit of our observations. The extremely low value of the predicted luminosity is mainly due to the great difference (by a factor of 11.7) of the periods.

On the other hand, apparently similar nonthermal optical radiation has been observed from Geminga (Bignami et al. 1988a; Halpern & Tytler 1988; Bignami et al. 1996)[8] whose period, age, and period derivative are not strongly different from those of B0656+14 (see, e.g., Goldoni et al. 1995), and whose optical flux is also too bright to be explained by the model of Pacini & Salvati. This means that the latter model is inapplicable to at least the middle-aged pulsars. An analysis of the dependence of

[7] The disagreement of the V flux from the B0656+14 candidate with the Pacini law has also been noticed by Caraveo et al. (1994a).

[8] This similarity allows us to predict a similar rise of the Geminga's spectrum in the far-UV domain which should be dominated by thermal radiation from the NS atmosphere. Moreover, the near-UV flux detected by Bignami et al. (1996) should be significantly contributed from the thermal component.

the optical efficiencies, $\eta_{opt} = L_{opt}/\dot{E}$, on the pulsar parameters for the five pulsars observed at optical wavelengths (Goldoni et al. 1995) shows the most smooth dependence on $\dot{P}$; η_{opt} generally grows with $\dot{P}$ (roughly, $\propto \dot{P}^2$). However, the physical reason for this dependence remains unclear. Quantitative models for nonthermal optical radiation of the isolated NSs have not been developed yet. The most popular qualitative models attribute the high-frequency (infrared to γ-ray) emission to the noncoherent curvature or synchrotron radiation from relativistic electrons near the velocity-of-light cylinder (e.g., Lyne & Graham-Smith 1990; Michel 1991, and references therein). In these models the UV-optical radiation is emitted at the same place and in the same direction as γ-rays, generally different from the direction of the radio emission which is produced above the magnetic poles near the NS surface. This hypothesis could explain why Geminga's optical and γ-ray, but not radio, radiation is observed. However, it is inconsistent with observations of B0656+14, which is detected in the UV-optical and *radio* domains, but not in γ-rays (Ulmer 1993; Hermsen et al. 1994). This implies that the simple model is again in need of revision, in particular, the revised model should explain the paucity of γ-radiation from B0656+14.

To develop adequate models of the nonthermal radiation, further multiwavelength observations of a larger sample of isolated NSs, particularly UV-optical spectral coverage, are needed. Until now, only the Crab pulsar spectrum has been analyzed in this range. Using the *HST* High Speed Photometer, Percival et al. (1993) found the extinction corrected Crab spectrum to be essentially flat in the range 1700–7300 Å: $F_\nu \propto \nu^{-\alpha}$ with $\alpha = -0.11 \pm 0.13$. Although the apparent slope of the spectrum of B0656+14 may be close to this, it is not clear whether this means that the same mechanism is responsible for the UV-optical radiation emitted by these two pulsars, the properties of which are quite different.

From the aforementioned trend of decreasing optical nonthermal efficiencies with $\dot{P}$, we would expect the UV-optical efficiency η_{130LP} for B0656+14 to be greater than those of B1929+10 and B0950+08 by factors of $\sim 2 \times 10^3$ and $\sim 6 \times 10^4$, respectively. The observed ratio of the B0656+14 to B0950+08 efficiencies is at least 4 orders of magnitude lower, which strengthens our conclusion (1*c*) that the detected radiation of B0950+08 is thermal. The ratio of the B0656+14 to B1929+10 efficiencies is much less certain because of the poorly known distances; its maximum value might be $\sim 10^3$ in the most extreme case, but about two orders of magnitude lower for more plausible distances. Thus, a considerable nonthermal component can hardly be expected in the optical-UV radiation from B1929+10.

The temperatures inferred for these old pulsars look also rather high compared to those predicted by NS cooling theories which do not include possible heating mechanisms. According to these theories, the surface temperature falls below 10^5 K when the NS reaches an age of $\sim(1\text{–}3) \times 10^6$ yr. However, various reheating processes may become important for the old NSs. In particular, internal heating due to dissipation of energy of differential rotation between the NS crust and more rapidly rotating interior superfluid was considered by Shibazaki & Lamb (1989), Umeda et al. (1993), and Van Riper et al. (1994). The amount of heat released depends on the value of the differential angular momentum J of the frictionally coupled superfluid layers, the NS mass and radius, an assumed equation of state, and the internal composition. Assuming the radiation from B0950+08 is thermal in origin, a comparison between our (bolometric) luminosity with the models computed by Umeda et al. (1993) for $M = 1.4\ M_\odot$, yields $J \sim (0.3\text{–}3) \times 10^{42}$ and $(0.3\text{–}3) \times 10^{44}$ g cm^2 rad s^{-1} for the extreme models with the hardest (PS; $R = 16.1$ km) and softest (BPS; $R = 7.9$ km) equations of state, respectively. Corresponding ranges of the critical angular velocity for unpinning of the superfluid vortices from the crust lattice are also quite different: $\omega_{cr} \sim 0.001\text{–}0.01$ rad s^{-1} (superweak pinning) and 0.7–7 rad s^{-1} (strong pinning), respectively. An independent estimate of ω_{cr} (e.g., from the analysis of the postglitch behavior of pulsars; Alpar et al. 1984), could determine which of these models better corresponds to real NSs. Note that in the latter case (strong pinning; BPS equation of state) a frictional instability may set in at an NS age of $\sim 10^7\text{–}10^9$ yr, which leads to oscillations of the surface temperature (Shibazaki & Mochizuki 1995). Although less certain, similar estimates for J and ω_{cr} are obtained for B1929+10 if $d \simeq 150\text{–}180$ pc.

Other internal heating mechanisms, e.g., Ohmic decay of the internal magnetic field in NSs (Haensel, Urpin, & Yakovlev 1990; Shalybkov 1994, and references therein) and deviation from chemical equilibrium the NS core due to NS spin-down (Reisenegger 1995), are expected to be less important than frictional heating in the pulsars under discussion.

The mechanisms discussed above delay the NS cooling but they cannot prevent it: an NS cools down with time. There may exist, however, a more exotic mechanism, nucleon decay caused by superheavy magnetic monopoles captured by the NS, which results in the NS luminosity linearly growing with time, so that one could expect a very old NS to become *hotter* (Freese, Turner, & Schramm 1983; Kolb & Turner 1984). The heating rate depends on the (unknown) Galactic monopole flux F_G. If we assume that the radiation from the older B0950+08 is completely provided by monopole-induced nucleon decay and make the same assumptions as Freese et al. (1983) regarding the cross section, monopole velocity, etc., then the flux estimated from the thermal luminosity estimate is $F_G \sim 10^{-24}$ cm^{-2} sr^{-1} s^{-1}. This flux (~ 1 monopole per $\sim 10^6$ km^2 yr^{-1}) is approximately 3 orders of magnitude lower than the upper limit obtained by Freese et al. (1983) from the *Einstein* observations of B1929+10. Our estimate for F_G is comparable to the upper limit obtained by Edelstein, Foster, & Bowyer (1995) from *EUVE* observations of the older (by a factor of 300) binary millisecond pulsar PSR J0437−4715. Edelstein et al. interpreted the *EUVE* flux as thermal radiation from the NS surface with $T_\infty^{bb} = (1.6\text{–}4.0) \times 10^5$ K and used the highest value of the temperature to estimate the upper limit on F_G. If their interpretation is correct, then indeed we can expect that cooling of NSs is replaced by heating after some age, and no other heating mechanism except the monopole capture is known to explain such behavior. If we accept this hypothesis, B0950+08 may be just at the beginning of this heating stage, or near the minimum of the cooling/heating curve. Heating induced by monopole catalysis scales with the pulsar age, $T^4 \propto \tau$. Extrapolating the temperature obtained from the *EUVE* observations of J0437−4715 to the younger age of B0950+08 yields $T_\infty^{bb} = (4\text{–}10) \times 10^4$ K, which is also compatible with our observation. Thus, its temperature can be

explained by either frictional or monopole heating, or both. To elucidate the situation, additional old pulsars should be observed at UV-optical and EUV wavelengths.

Heating of the NS surface can be also caused by the bombardment of the magnetic pole regions with ultrarelativistic particles and γ-rays created above the poles of active pulsars. The energy of the particles and photons is released in the (optically thick) surface layers and transferred outward by heat conduction. As discussed above, the radiation from the hot polar cap is itself too faint in the UV-optical range to be detected because of its small area. The heat transfer along the NS surface could increase the temperature of a larger surface area. The efficiency of this mechanism depends on the poorly known heat conductivity in the relatively cold, strongly magnetized outer NS crust. It has not been investigated in sufficient detail for a quantitative analysis to be made.

Some additional reheating could be, in principle, caused by accretion of interstellar matter onto the NS surface provided the NS velocity through the ISM is sufficiently slow (e.g., Treves & Colpi 1991; Zane et al. 1995, and references therein). In the case of isotropic accretion, when the entire NS surface is heated, an effective surface temperature of $\sim 10^5$ K can be maintained by a quite modest accretion rate, $\dot{M} = 8.4 \times 10^8 R_{13}^3 (M/1.4\ M_\odot)^{-1} T_5^4$ g s^{-1}, which corresponds to an accretion luminosity of $L = 8.6 \times 10^{28}$ ergs s^{-1}. However, this accretion rate can be achieved only for velocities $v < 60 R_{13}^{-1} (M/1.4\ M_\odot)^{1/3} (n/1\ \mathrm{H\ cm^{-3}})^{1/3} T_5^{-4/3}$ km s^{-1}, where n is the hydrogen number density in the interstellar medium. The pulsars under discussion have velocities larger than this. Besides, their magnetic fields are high enough to channelize accretion onto a much smaller area around the magnetic poles, which increases the effective temperature (at the same $\dot{M}$ and L) but *decreases* the UV-optical flux. In addition, active pulsars should hamper or even prevent accretion, a problem which requires additional investigation.

Finally, if we assume that conclusion (2) is correct and the objects we detected are *not* the pulsars, very stringent limits can be placed on the cooling/heating models and NS parameters. For B0656+14 it would mean that $T_\infty^{\mathrm{bb}} < 1 \times 10^5$ K, which, although it could be obtained from very "nonstandard" cooling models, would be inconsistent with the *ROSAT* results. B0950+08 would have an unprecedented low temperature, $T_\infty^{\mathrm{bb}} < 3 \times 10^4$ K for its minimum distance and maximum radius, which would mean very low values for the differential angular momentum, $J \lesssim 10^{40}$ and $\lesssim 10^{42}$ g cm^2 rad s^{-1} for the hardest and softest equations of state, respectively. It would also put an upper limit on the magnetic monopole flux, $F_G < 10^{-26}$ cm^{-2} sr^{-1} s^{-1}, two orders of magnitude lower than the estimate obtained assuming that B0950+08 was detected. Such a low temperature would be difficult to reconcile with that obtained from the much older J0437−4715.

Support for this work was provided by NASA through grant GO-5377.01-93A from the Space Telescope Science Institute, which is operated by the Association of Universities for Research in Astronomy, Inc., under NASA contract NAS 5-26555. We are very grateful to Diane Gilmore, Paul Greenfield, Warren Hack, Bob Jedrzejewski, Brian McLean, Krista Rudloff, Bernie Simon, Peg Stanley, Denise Taylor, and Deborah Wallace of the STScI for their assistance in carrying out these observations and for discussions regarding data reduction and the detector characteristics. G. P. thanks Slava Zavlin for his assistance with computing the NS atmosphere models, Reed Meyer for collaboration in fitting of the *ROSAT* spectra of pulsars, Dima Yakovlev for useful discussions of the NS cooling theories, and Yurii Gnedin for his participation in preparation of the first version of the proposal to observe NSs with *HST*. We are grateful to the referee, Patrizia Caraveo, for sending us the paper of Bignami et al. (1996) prior to publication.

REFERENCES

Alpar, M. A., Anderson, P. W., Pines, D., & Shaham, J. 1984, ApJ, 276, 325
Anderson, S. B., Córdova, F. A., Pavlov, G. G., Robinson, C. R., & Thompson, R. J. 1993, ApJ, 414, 867
Aoki, S., Soma, M., Kinoshita, H., & Inoue, K. 1983, A&A, 128, 263
Arzoumanian, Z., Nice, D. J., Taylor, J. H., & Thorsett, S. E. 1994, ApJ, 422, 671
Backer, D. C., & Sramek, R. A. 1981, in Pulsars, ed. W. Sieber & R. Wielebinski (Dordrecht: Reidel), 205
———. 1982, ApJ, 260, 512
Becker, W., & Aschenbach, B. 1995, in The Lives of the Neutron Stars, ed. M. A. Alpar, Ü. Kiziloğlu, & J. van Paradijs (Dordrecht: Kluwer), 47
Bertsch, D. L., et al. 1992, Nature, 357, 306
Bignami, G. F., Caraveo, P. A., Mignani, R., Edelstein, J., & Bowyer, S. 1996, ApJ, 456, L111
Bignami, G. F., Caraveo, P. A., & Paul, J. A. 1988a, A&A, 202, L1
Bignami, G. F., Caraveo, P. A., Paul, J. A., Salotti, L., & Vigroux, L. 1987, ApJ, 319, 358
Bignami, G. F., Caraveo, P. A., & Vacanti, G. 1988b, A&A, 196, 191
Caraveo, P. A., Bignami, G. F., & Mereghetti, S. 1994a, ApJ, 422, L87
Caraveo, P. A., Bignami, G. F., Mereghetti, S., & Mombelli, M. 1992, ApJ, 395, L103
Caraveo, P. A., Mereghetti, S., & Bignami, G. F. 1994b, ApJ, 423, L125
Córdova, F.A., Hjellming, R. M., Mason, K. O., & Middleditch, J. 1989, ApJ, 345, 451
Córdova, F. A., Stringfellow, G. S., & Pavlov, G. G. 1994, BAAS, 26, 889
Dewey, J., Taylor, J. H., Maguire, C. M., & Stokes, G. H. 1988, ApJ, 332, 762
Dickey, J. M., Weisberg, J. M., Rankin, J. M., & Boriakoff, V. 1981, A&A, 101, 332
Downes, G. S., & Reichley, P. E. 1983, ApJS, 53, 169
Edelstein, J., Foster, R. S., & Bowyer, S. 1995, ApJ, 454, 442
Fanselow, J. L., Sovers, O. J., Thomas, J. B., Purcell, G. H., Cohen, E. J., Rogstad, D. H., & Skjerve, L. G. 1984, AJ, 89, 987
Finley, J. P. 1994, in AIP Conf. Proc. 313, The Soft X-Ray Cosmos, ed. E. Schlegel & R. Petre (New York: AIP), 41
Finley, J. P., Ögelman, H., & Kiziloğlu, Ü. 1992, ApJ, 394, L21
Fomalont, E. B., Goss, W. M., Lyne, A. G., & Manchester, R. N. 1984, MNRAS, 210, 113
Fomalont, E. B., Goss, W. M., Lyne, A. G., Manchester, R. N., & Justtanont, K. 1992, MNRAS, 258, 497
Foster, R. S., Edelstein, J., & Bowyer, S. 1996, in IAU Colloq. 152, Astrophysics in the Extreme Ultraviolet, ed. S. Bowyer & R. Malina (Dordrecht: Kluwer), 437
Freese, K., Turner, M. S., & Schramm, D. N. 1983, Phys. Rev. Lett., 51, 1625
Fruscione, A., Hawkins, I., Jelinsky, P., & Wiercigroch, A. 1994, ApJS, 94, 127
Goldoni, P., Musso, C., Caraveo, P. A., & Bignami, G. F. 1995, A&A, 298, 535.
Gwinn, C. R., Taylor, J. H., Weisberg, J. M., & Rawley, L. A. 1986, AJ, 91, 338
Hack, W. 1994, STScI Instrum. Sci. Rep. FOC-081
Hack, W., & Nota, A. 1994, STScI Instrum. Sci. Rep. FOC-080
Haensel, P., Urpin, V. A., & Yakovlev, D. G. 1990, A&A, 229, 133
Halpern, J., & Holt, S. S. 1992, Nature, 357, 222
Halpern, J., & Ruderman, M. 1993, ApJ, 415, 286
Halpern, J., & Tytler, D. 1988, ApJ, 330, 201
Hermsen, W., et al. 1994, ApJS, 92, 559
Kolb, E. W., & Turner, M. S. 1984, ApJ, 286, 702
Kristian, J. 1970, ApJ, 162, L173
Lyne, A. G., Anderson, B., & Salter, M. J. 1982, MNRAS, 201, 503
Lyne, A. G., & Graham-Smith, F. 1990, Pulsar Astronomy (Cambridge: Cambridge Univ. Press)
Ma, C., Shaffer, D. B., de Vegt, C., Jonston, K. J., & Russel, J. L. 1990, AJ, 99, 1284
Manchester, R. N., et al. 1978, MNRAS, 184, 159

Manning, R. A., & Willmore, A. P. 1994, MNRAS, 266, 635
Mereghetti, S., Caraveo, P. A., & Bignami, G. F. 1994, ApJS, 92, 521
Meyer, R. D., & Pavlov, G. G. 1993, unpublished
Meyer, R. D., Pavlov, G. G., & Mészáros, P. 1994, ApJ, 433, 265
Michel, F. C. 1991, Theory of Neutron Star Magnetospheres (Chicago: Univ. Chicago Press)
Middleditch, J., & Pennypacker, C. 1985, Nature, 313, 659
Nota, A., Jedrzejewski, R., & Hack, W. 1995, Faint Object Camera Instrument Handbook [Post-COSTAR], Version 6.0, June 1995
Ögelman, H. 1995, in The Lives of the Neutron Stars, ed. M. A. Alpar, Ü. Kiziloğlu, & J. van Paradijs (Dordrecht: Kluwer), 101
Pacini, F. 1971, ApJ, 163, L17
Pacini, F., & Salvati, M. 1987, ApJ, 321, 447
Pavlov, G. G., Shibanov, Yu. A., Zavlin, V. E., & Meyer, R. D. 1995, in The Lives of the Neutron Stars, ed. M. A. Alpar, Ü. Kiziloğlu, & J. van Paradijs (Dordrecht: Kluwer), 71
Percival, J. W., et al. 1993, ApJ, 407, 276
Perriman, M. A. C., et al. 1989, A&A, 215, 195
Peterson, B. A., et al. 1978, Nature, 276, 475
Reisenegger, A. 1995, ApJ, 442, 749
Salter, M. J., Lyne, A. G., & Anderson, B. 1979, Nature, 280, 461
Savage, B. D., & Mathis, J. S. 1979, ARA&A, 17, 73
Shalybkov, D. A. 1994, Astron. Lett., 20, 182
Shibazaki, N., & Lamb, F. K. 1989, ApJ, 346, 808
Shibazaki, N., & Mochizuki, Y. 1995, ApJ, 438, 288
Siegman, B. C., Manchester, R. N., & Durdin, J. M. 1993, MNRAS, 262, 449
Stringfellow, G. S, Pavlov, G. G., & Córdova, F. A. 1994, BAAS, 26, 1441
Taff, L. G., et al. 1990, ApJ, 353, L45
Taylor, J. H., Manchester, R. N., & Lyne, A. G. 1993, ApJS, 88, 529
Thompson, R., J., & Córdova, F. A. 1994, ApJ, 421, L13
Treves, A., & Colpi, M. 1991, A&A, 241, 107
Ulmer, M. P. 1993 ApJS, 90, 789
Umeda, H., Shibazaki, N., Nomoto, K., & Tsuruta, S. 1993, ApJ, 408, 186
Van Riper, K. A. 1991, ApJ, 372, 251
Van Riper, K. A., Link, B., & Epstein, R. J. 1994, ApJ, 448, 294
Weisberg, J. M., Rankin, J. M., & Boriakoff, V. 1980, A&A, 88, 84
Yancopoulos, S., Hamilton, T. T., & Helfand, D. 1994, ApJ, 429, 832
Zane, S., Turolla, R., Zampieri, L., Colpi, M., & Treves, A. 1995, ApJ, 451, 739